Review

Not peer-reviewed version

# An Overview of Solid Fuel Processing, Kinetics, and the Advances in Minimizing Carbon Monoxide Emissions

ANTONY NYOMBI *, Mike Williams , Roland Wessling

Posted Date: 10 October 2023

doi: 10.20944/preprints202310.0528.v1

Keywords: Pyrolysis; combustion emissions; improved cookstoves; advanced boilers; CO detectors; catalyst impregnation

*Review*

# An overview of solid fuel processing, kinetics, and the advances in minimizing Carbon monoxide emissions

**Nyombi A [1,*], Williams M R [2] and Wessling R [1]**

[1] Cranfield Forensic Institute – Cranfield University – Shrivenham. Defence Academy of the United Kingdom. SN6 8LA - United Kingdom
[2] Center for Defence Chemistry - Cranfield University – Shrivenham. Defence Academy of the United Kingdom. SN6 8LA - United Kingdom
* Correspondence: antonynyombi@gmail.com

**Abstract:** There is a growing notion that biomass are the best resource to replace the declining fossil fuels, yet both share the long lived human threat: toxic combustion emissions. Among the toxic combustion products is carbon monoxide (CO) that not only causes acute but also chronic ailments. This brief review discusses the solid fuel processing technologies from combustion, thermochemical and biochemical processing to kinetics and thermodynamics including the mechanism for release of CO. It further expounds on the burden that CO has caused England and Wales in the last 25 years. The main gist are the systems that have been developed to minimize human exposure to CO including cooking, heating, catalytic and detection systems. Finally, alternative technologies are discussed that work by changing the chemical nature of solid fuels as a way to minimize CO emissions.

**Keywords:** pyrolysis; combustion emissions; Improved cookstoves; advanced boilers; CO detectors; catalyst impregnation

## Highlights

- Solid fuel processing methods are discussed including extensive analysis of kinetics and thermodynamics
- Emission of pollutants from solid fuels is examined
- Mechanism for release of carbon monoxide (CO) is outlined
- Detailed analysis of systems used for minimizing human exposure to CO
- Recommendations for better methods used to process solid fuels especially those used for cooking are discussed

## 1. Introduction

It is of great importance that the emission of toxic gases from the combustion of solid fuels is minimised while diversifying energy sources to supplement the declining fossil fuels. Wood and coal are regarded as the world's most used solid fuels in homes (Ots et al., 2018), (Char and Graphite, 2017). It is estimated that 90% of solid fuel (coal, crop residue, and woody materials) consumption is by developing countries. This population constitutes more than three billion people (Shen et al., 2014). Biomass is the best foreseeable solid fuel to replace coal due to its ease of processing, friendliness to the environment and abundance.

Based on biological variety, biomass may be classified as wood like barks, conifers, stems, angiosperm, chips, sawdust, softwood, pellets (Sikarwar et al., 2017). These contain very low levels of contaminants (heavy metals and sulfur) and are easily processed by conventional methods like co-firing, combustion, cogeneration, gasification, and torrefaction. Biomass may also be herbaceous and agricultural to include straws like wheat, corn, rice, barley; flowers and grasses including

 doi:10.20944/preprints202310.0528.v1



switchgrass, bamboo and cane and other residues like pulp, husks, grains, bagasse, and shells. Marine life like micro-organisms and plants like algae, water hyacinth, and weed also have a high potential for bioenergy. Industrial and contaminated waste like refuse-derives fuels, sewage sludge, municipal solid waste, plywood, paper-pulp sludge may also be used as bioenergy sources.

In the UK, the main biomass materials include palm, soya and sunflower oils, sugarcane, and palm or coconut husks (Anderson and Fergusson, 2006). Other solid fuels may be formed from food waste which comprises approximately 10 million tonnes. Most of this is discarded annually in the UK of which only 18% was recycled in 2016 (Nyombi et al., 2019). Charcoal derived from pyrolysis of carbonaceous materials is widely used as a fuel for home, industrial and recreational energy generation purposes. Coal is one of the oldest carbon rich solid fuel. There are four types of coal including peat, lignite, bituminous, and anthracite, with anthracite being most desirable due to its high heat content (Lisandy et al., 2017).

High volatile matter content and moisture render biomass a low energy intensive fuel. Processing such solid fuels is necessary to enhance energy output, reduce toxic and ozone depleting emissions and to increase the share of certain products in the outputs (i.e. gasification for increased gaseous products and bio-oil, torrefaction and low temperature pyrolysis for generating high quality solid products (Wang and Howard, 2018), etc.). During the processing of solid fuels, they undergo certain reaction mechanisms depending on the material properties and the controls used in the process. The data produced from controlled processing are used to determine the kinetic parameters for the processing or usage of solid fuels. The energy variations of enthalpies of activation between the reagent and the activated complex are usually in accordance with activation energies. Such properties are used to assess a given solid fuels for bioenergy production (M. S. Ahmad et al., 2017), (Lee et al., 2017), (Muktham et al., 2016).

During processing or usage of solid fuels, the main evolved gases are usually CO, $CO_2$, $H_2O$, $CH_4$, and $C_2H_4$ (Malika et al., 2016), (Özsin and Pütün, 2017). The production of CO, $H_2$, and $CO_2$ is enhanced under $CO_2$ (Borrego et al., 2009), over $N_2$, Ar, or air atmospheres. Pyrolysis enhances the carbon mass fraction while $H_2$, $O_2$, $N_2$ and S mass fractions are reduced (Sadaka et al., 2015).

The smoke from burning solid fuels especially coal contains fine particles, CO, benzene, polycyclic aromatic hydrocarbons (PAHs) among other pollutants which are associated with reduced intrauterine growth (Adrian, 2011). Carbon monoxide has always posed serious dangers to human life. The lungs of mummified bodies from the Paleolithic era are frequently black (Borsos et al., 2003), a sign of heavy smoke which is indicative of poor combustion and thus CO production. In 1850's Claude Benard showed that CO blocked respiration in erythrocytes (Russell and Jeraci, 1984). Even in ruminants, CO is reported to decrease the digestion of hemicellulose and cellulose by 40 and 27% respectively (Russell and Jeraci, 1984).

In the effort to reduce toxic and greenhouse gas emissions, the EU through its European decarbonisation strategy 2050, has set targets including the 22% of the energy share should come from renewables by 2030 and 42% by 2050 up from 9% in 2010 (Capros et al., 2014). Furthermore, there are available technologies for minimizing CO including sensors (Nandy et al., 2018), improved cookstoves (Lucarelli et al., 2018), better heating systems (Ozil et al., 2009), catalytic systems (Carltonbird et al., 2018), (Hong and Sun, 2016) among others.

The objectives of this work therefore are to give an overview of the major solid fuel processing technologies, kinetics and the major emissions with focus on carbon monoxide (CO) (section 3). Furthermore, technologies for minimizing CO exposure to humans have been listed and explained in detail (section 4). Finally, impregnation of chemical substances into solid fuels (section 5) is discussed as a way to influence certain reactions to produce desired products.

## 2. Methodology

This work is neither a comprehensive nor a systematic review. It is an attempt to give a general overview of solid fuel processing, toxic combustion emissions, and the major systems used to minimize human exposure to toxic pollutants under a three-pillar approach:

a. To succinctly delineate the solid fuel processing technologies including combustion, thermochemical and biochemical processing; give an account on the solid fuel combustion kinetics; and elucidate on the burden associated with combustion emissions with focus on carbon monoxide,
b. To list the major systems that have been used to minimize human exposure to carbon monoxide emissions from solid fuel combustion
c. To briefly justify the chemical changes imparted by use of chemical impregnation methods on solid fuel combustion

The methodical approach to this review was three-fold:

i. The solid fuel processing technologies, combustion kinetics and the challenge brought by CO poisoning was delineated. The authors carefully studied the relevant literature in relation to solid fuel combustion (i.e. smoldering, flaming), thermochemical conversion (torrefaction, flash carbonization, pyrolysis, gasification, hydrothermal, and liquefaction), and biochemical conversion technologies. They further collected literature on solid fuel combustion kinetics including the mechanisms for release of emissions, and kinetic parameters. Finally, the authors enumerated the challenges brought by CO poisoning including statistics on death by year in England and Wales.
ii. The major systems used to minimize human exposure to CO are listed and briefly explained. These included, improved cookstoves, heating systems, catalytic oxidation systems and CO detection systems
iii. The authors also briefly highlight the importance of using chemical catalysts as additives to solid fuels to be used for various applications.

Collecting the data involved examining scientific literature (Scopus, Google scholar, Science Direct) and "other" literature including industrial work, and commercial literature as empirical articles or theoretical. The key words used either individually or in combinations included; solid fuel; combustion, thermochemical conversion; biochemical conversion; combustion kinetics; combustion emissions; cookstoves, heating systems; CO oxidation; CO sensors; catalyst impregnation.

## 3. Solid fuel processing, kinetics, and CO emissions

### *3.1. Solid fuel processing technologies*

#### 3.1.1. Combustion

Combustion may be smoldering, flaming or a combination of both. The occurrence of any type depends on the prevailing conditions, usually temperature, airflow, and material properties.

Smoldering

Smoldering is a low-temperature, slow, flameless combustion maintained by heat from the reaction of oxygen with fuel components (Rein, 2016). It involves both pyrolysis of the original fuel and oxidation of the resulting char. Since smoldering usually occurs in limited oxygen supply, the rate of reaction is directly proportional to the oxygen mass flux. At above 35% oxygen supply, smoldering may transition to flaming (Hadden et al., 2013). This transition may also occur at temperatures just above 450 $^{o}$C in sawdust materials (Nyombi et al., 2019). For sawdust and charcoal, smoldering is affected by temperature, ash content, volatile matter content, particle size oxygen supply, and heat loss. With sawdust, temperature increases while during charcoal smoldering, temperature decreases. Low ash content allows oxygen diffusion leading to increased smoldering front propagation. High volatile content fuels produce much smoke during smoldering compared to low volatile content fuels (He et al., 2014).

Preprints (www.preprints.org) | NOT PEER-REVIEWED | Posted: 10 October 2023 doi:10.20944/preprints202310.0528.v1



If smoldering starts from the top, the fire will usually spread sideways and downwards Figure 1. This creates a void in the form of a pan semi-filled with ash. The downward spread is facilitated by forward smoldering. The sideways/lateral fire spread is enhanced by oxygen availability and is usually faster than downward smoldering due to ash and char layers that prevent quick penetration of oxygen during the downward flow. Under the natural conditions, the flow induced by the plume ensures sufficient oxygen supply to sustain the horizontal spread of fire to the top-most layer. Oxygen then penetrates by diffusion (Rein, 2016).

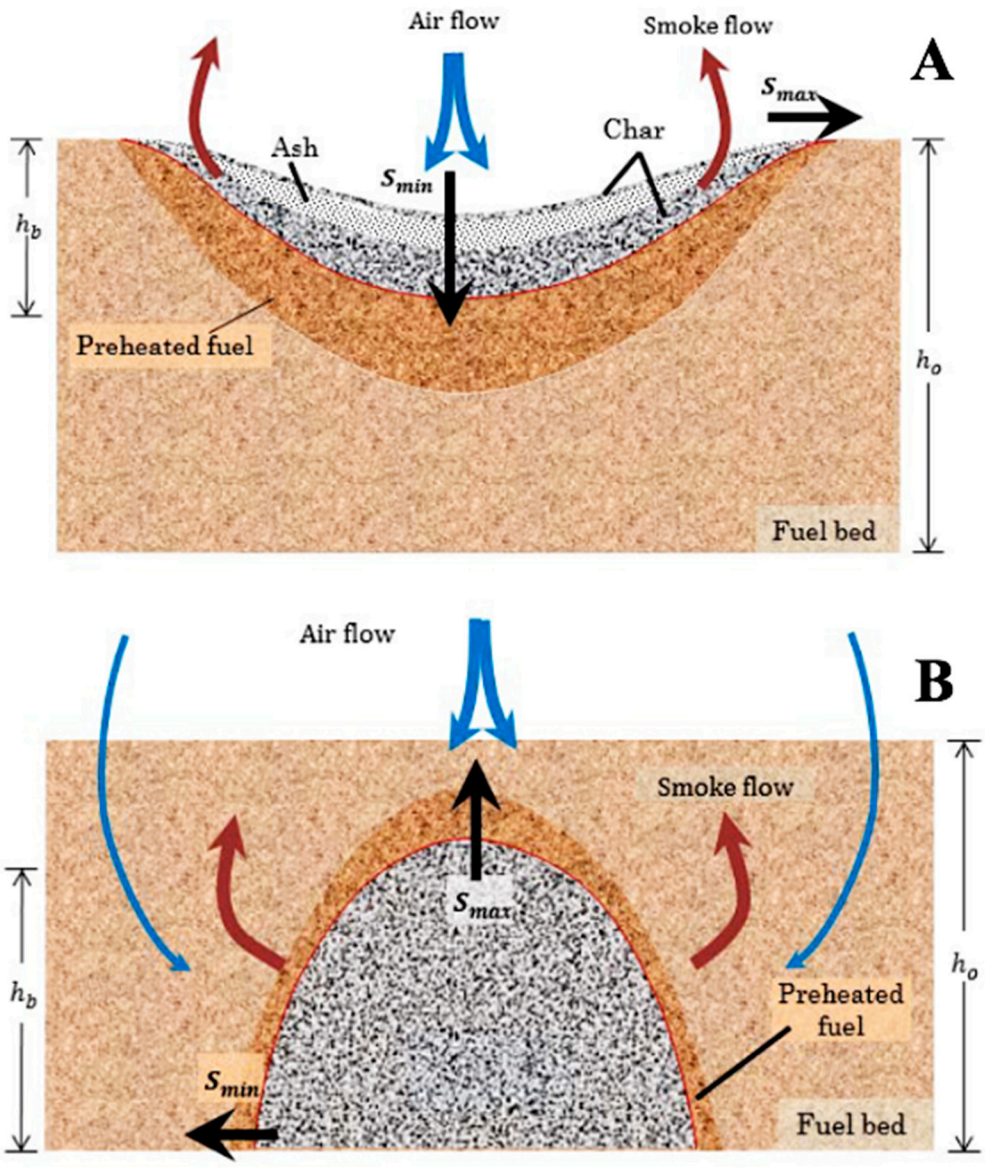


**Figure 1.** Downward (A) and upward (B) smoldering propagation in a porous solid fuel. Adapted and modified from (Rein, 2016).

Flaming

Flaming combustion is the process occurring when visible flames and plume of a fire are visible. A flame is the visible, luminous body where the oxidation reaction is occurring. In flaming combustion, the fuel is in the gas phase. The reactions and heat release occur in the gas adjacent to the liquid or solid surface. Flaming combustion is controlled by external and internal factors (Moghtaderi and Fletcher, 1998). External factors include the temperature and oxygen

 doi:10.20944/preprints202310.0528.v1



availability, as well as the radiant heat flux. The internal factors include the moisture content and the geometrical properties.

3.1.2. Thermochemical processing

Torrefaction

Torrefaction (Chen et al., 2015) is a low temperature (200–300 °C) process in an inert environment in which moisture, carbon oxides (CO & $CO_2$), and oxygen are removed from biomass materials including depolymerisation of long-chain polysaccharide forming a solid product with low H/C and O/C ratios. Several studies (Sun et al., 2016) (Weber and Quicker, 2017), (Varjani et al., 2019) have shown that the properties of the final product (weight loss, thermophysical and chemical) are influenced mainly by torrefaction temperature. High temperatures favour biochar while bio-oil decreases. The non-condesable gases remain almost constant (Chen et al., 2015). Torrefaction is aimed at improving the thermochemical properties of final biomass product for application in co-firing with coal, gasification, and combustion.

Flash carbonization

This is a high-pressure process (1-2 Mpa) in which a flash fire ignited on a biomass packed bed results in a solid and gas-phase as the main products. Flash carbonisation is usually operated at mid-level temperatures (300-600 °C) and short residence time in the range of 30-40 minutes. About 40% yield is a solid product. This process is not very much embraced compared to other methods for making biochar (Chen et al., 2015).

Pyrolysis

Pyrolysis is a slow breakdown of organic matter contained in solid fuel at temperatures 300-900 °C under limited oxygen conditions. In biomass solid fuels, the main constituents (cellulose, hemicellulose, and lignin) each undergoes separate reaction routes including depolymerisation, cross-linking and fragmentation at appropriate temperatures. The main products of pyrolysis are solid (char), liquid (bio-oil) and gaseous (syngas - CO, $CO_2$, $H_2$, and $C_1$–$C_2$ hydrocarbons). The quantity and quality of each product depend on the pyrolysis conditions (heating rate, final holding temperature and residence time) and the properties of the raw materials used (Sun et al., 2016), (Weber and Quicker, 2017), (Brennan and Owende, 2010). Generally, syngas increases while biochar decreases with increasing pyrolysis temperature (Sun et al., 2016).

Gasification

Gasification is a high temperature (800-1000 °C) process in which biomass is partially oxidised using air, steam, oxygen, $CO_2$ or gas mixture, forming gaseous products mainly CO, $H_2$, $CO_2$, N, and $CH_4$. Other products include biochar which is usually 5-10% of the starting raw material and liquid products (tar & oils). Gasification can produce syngas from a wide variety of raw materials (biomass, coals, and plastics), unlike other similar processes. Much as syngas has a low calorific value ( 4–6 MJ $m^3$), it can burn directly or be used as a fuel for gas turbines and engines (Sun et al., 2016), (Weber and Quicker, 2017), (Varjani et al., 2019), (Brennan and Owende, 2010). The gasifiers used may be fixed bed reactors; moving bed reactors; fluidized bed reactors; or entrained bed reactors depending on the interaction between the biomass and the gasification agent. Gasification reactions are affected by the gasification agent type, reaction temperature, pressure, and gasification agent–biomass ratio. The reaction temperature is usually the main parameter influencing gasification reactions (Sun et al., 2016).

Hydrothermal

Unlike dry thermal processes (pyrolysis and gasification), hydrothermal processes involve mixing biomass with water and the product is left to stabilise in a reactor. After a certain period, the

Preprints (www.preprints.org) | NOT PEER-REVIEWED | Posted: 10 October 2023 doi:10.20944/preprints202310.0528.v1



temperature of the reactor is raised. To keep the water in the liquid phase, high pressures are used. This process may be called hydrothermal carbonisation if the main intended product is hydrochar; hydrothermal liquefaction for bio-oil; and hydrothermal gasification for syngas. Hydrochar usually has a high carbon content compared to dry processes (pyrolysis and gasification). In addition to heating rate, final holding temperature and residence time used in dry processes, the water-biomass ratio also plays a vital role to the final product yield (Varjani et al., 2019).

Liquefaction

Liquefaction is a high pressure (5-20 MPa), low temperature (300-350 °C) process used to convert high moisture content materials like algal biomass into liquid fuels (bio-oil). The process is aided by catalysts in the presence of hydrogen. Compared to other thermal processes, liquefaction is quite expensive and involves complex reaction systems (Brennan and Owende, 2010).

3.1.3. Biochemical processing

The biological process for energy conversion of biomass into other fuels includes anaerobic digestion, fermentation and photobiological hydrogen production (Brennan and Owende, 2010). Anaerobic digestion is mainly for the production of biogas (composed of $CH_4$ as the main product, $CO_2$ and nitrogen); fermentation is for production of bioethanol while photobiological hydrogen production, like the name suggests, is for $H_2$ production (Anderson and Fergusson, 2006), (Weber and Quicker, 2017).

Figure 2, summaries the different types of biomass processing technologies and the main products.

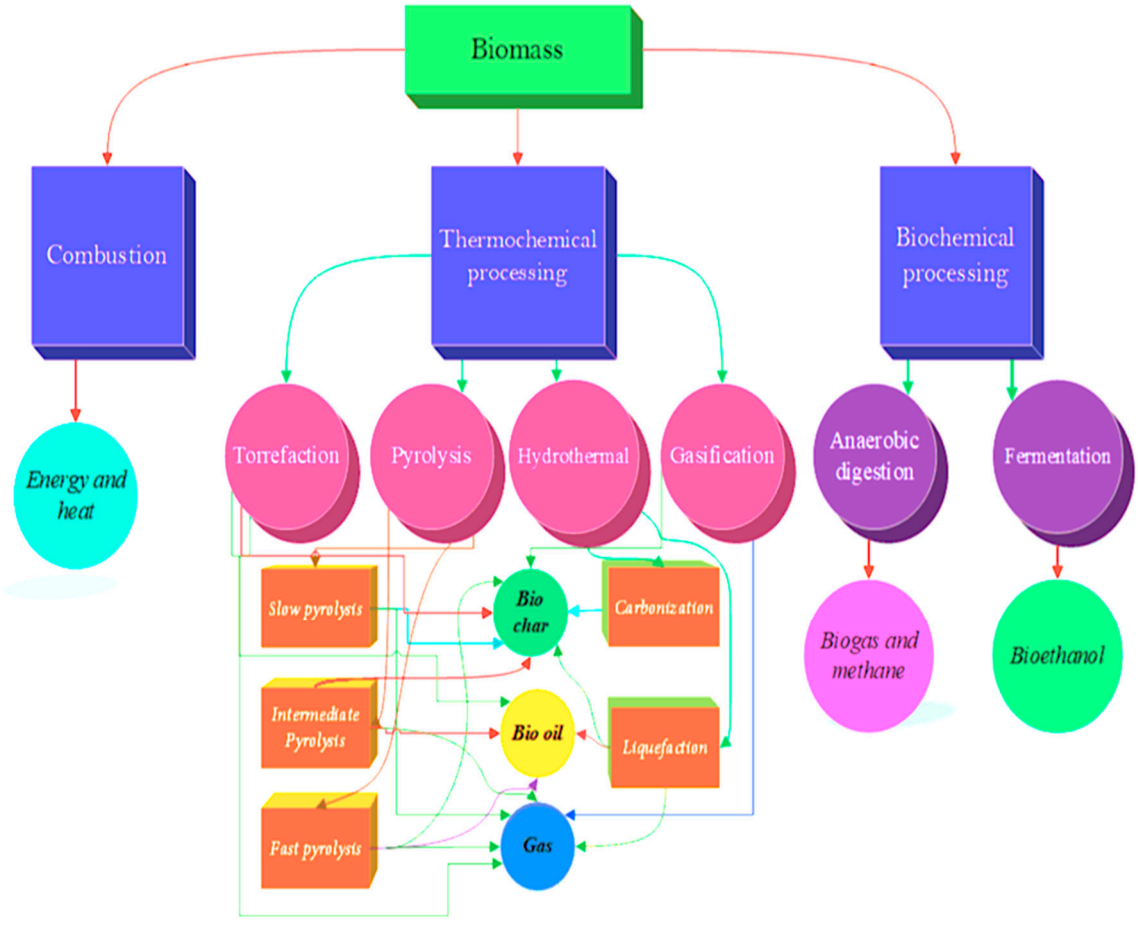


**Figure 2.** Biomass processing technologies and respective products obtained through each of the technologies (Akhtar et al., 2018).

Preprints (www.preprints.org) | NOT PEER-REVIEWED | Posted: 10 October 2023 doi:10.20944/preprints202310.0528.v1



*3.2. Solid fuel combustion kinetics*

3.2.1. General mechanism for release of emissions

Solid fuel combustion is a complex process involving simultaneous mass and heat transfer with chemical reactions. The prediction of solid fuel combustion for design, process analysis, and control demands an in-depth understanding of the fuel properties and how these will influence the final desired product (Jenkins et al., 1998). A general global reaction of solid fuel in the air might follow the reaction:

$$C_{x1}H_{x2}O_{x3}N_{x4}S_{x5}Cl_{x6}Si_{x7}K_{x8}Ca_{x9}Mg_{x10}Na_{x11}P_{x12}Fe_{x13}Al_{x14}Ti_{x15} + n_1H_2O + n_2\,(1+e)(O_2 + 3.7N_2) = n_3CO_2 + n_4H_2O + n_5O_2 + n_6N_2 + n_7CO + n_8CH_4 + n_9NO + n_{10}NO_2 + n_{11}SO_2 + n_{12}HCl + n_{13}KCl + n_{14}K_2SO_4 + n_{15}C + \cdots$$

The coefficients $x_1$-$x_{15}$ in hybrid poplar and rice straw may take the following values shown in Table 1.

**Table 1.** Proposed elemental coefficients of a typical biomass solid fuel (Jenkins et al., 1998).

| Element | Coefficient | Hybrid poplar | Rice straw | Rice/Poplar |
|---|---|---|---|---|
| C | $x_1$ | 4.1916 | 3.2072 | 0.77 |
| H | $x_2$ | 6.0322 | 5.1973 | 0.86 |
| O | $x_3$ | 2.5828 | 2.8148 | 1.09 |
| N | $x_4$ | 0.0430 | 0.0625 | 1.45 |
| S | $x_5$ | 0.0006 | 0.0057 | 9.50 |
| Cl | $x_6$ | 0.0003 | 0.0165 | 55.00 |
| Si | $x_7$ | 0.0057 | 0.5000 | 87.72 |
| K | $x_8$ | 0.0067 | 0.0592 | 8.84 |
| Ca | $x_9$ | 0.0337 | 0.0141 | 0.42 |
| Mg | $x_{10}$ | 0.0205 | 0.0135 | 0.66 |
| Na | $x_{11}$ | 0.0002 | 0.0079 | 39.50 |
| P | $x_{12}$ | 0.0012 | 0.0086 | 7.17 |
| Fe | $x_{13}$ | 0.0007 | 0.0029 | 4.14 |
| Al | $x_{14}$ | 0.0008 | 0.0073 | 9.13 |
| Ti | $x_{15}$ | 0.0002 | 0.0004 | 2.00 |

The 15 elements included in the empirical formula form just part of the complete biomass fuel composition. The metallic constituents are responsible for the ash content of a given solid fuel. The moisture term is responsible for the spontaneity of reactions during combustion. The simplified air term (21% oxygen and 79% nitrogen) has a significant meaning in that the presence of certain gases in the fuel may contribute heavily to the reaction progress in solid fuel combustion. The products are much more complex than what is shown in the equation above and the detailed chemistry varies considerably depending on the system (Jenkins et al., 1998).

3.2.2. Mechanisms for release of CO

The structures of functional groups that are present on the char or found on partially oxidized char surfaces are presented in Figure 3. These structures are responsible for the formation of CO in addition to the free-edge site reactions.

Preprints (www.preprints.org) | NOT PEER-REVIEWED | Posted: 10 October 2023 doi:10.20944/preprints202310.0528.v1



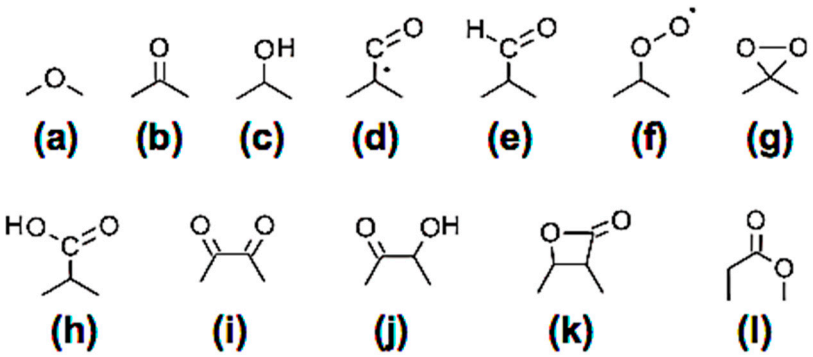


**Figure 3.** Several oxygenated functional groups present on partially oxidized PAHs or soot. (a) Pyrone (ether). (b) Ketone. (c) Hydroxyl. (d) Dangling CO (carbonyl). (e) Dangling HCO. (f) Peroxide. (g) Dioxyranyl. (h) Carboxylic. (i) Quinone. (j) Phenolic. (k) Lactone. (l) Oxypinyloxy (Raj et al., 2012), (A. Nyombi, M. Williams, 2019).

After the surface oxygenated functional groups are all oxidized, further reactions follow the "free edge site" reactions leading to formation of CO, a reaction similar to the breakdown of soot reported in the literature (Raj et al., 2012). This follows a simplified mechanism, though numerous reactive sites can be present. As seen in Figure 4, free-edge sites and zig-zag sites on a polycyclic aromatic hydrocarbon (PAH) molecule react with oxygen to release CO and the formation of new edge-sites. This process is repeated until all the edge-sites are completed, after which, complete oxidation of the six-membered rings takes place until the entire structure is oxidised (Raj et al., 2012).

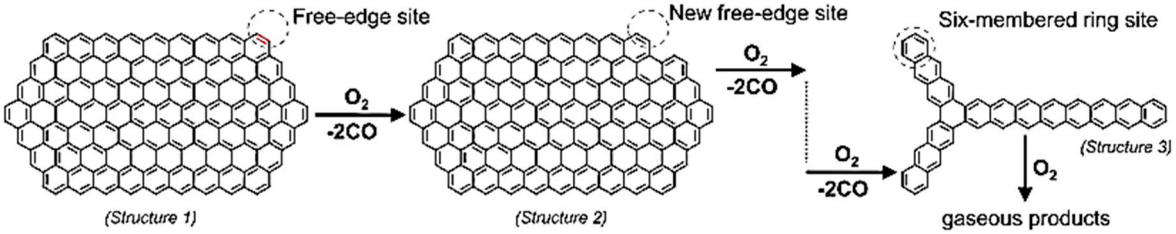


**Figure 4.** Free-edge oxidation of an example polycyclic aromatic hydrocarbon molecule comprising a soot particle. The oxidation of a free-edge on structure 1 leads to the generation of a new free-edge in this example on structure 2, thus causing chain oxidation through the reaction (Raj et al., 2012).

Further detailed complex reactions involve the breakdown of planar and curved PAHs which involves the formation of oxygenated free radicals that later desorb as CO or $CO_2$. Other carbon-centered free radicals react with oxygen forming CO as the main product (Raj et al., 2013), (Parker et al., 2015).

3.2.3. Kinetic parameters for pyrolysis or oxidation of solid fuels

The main methods that have been used over the years for the determination of activation energies during pyrolysis or oxidation reactions of solid fuels are here summarized in Table 2. The description and modelling of the reactions/mechanisms involved in solid fuel processing have been a serious challenge. This has been mainly due to multi-step and parallel reactions and the heterogeneous nature of solid fuels during decomposition. Hence researchers have developed model-fitting and model free iso-conversional as well as model methods to solve the challenge. These have been applied to TGA/DSC data and used to predict as accurate as possible the kinetic parameters during solid fuel decomposition. These can sometimes get complex for solid fuel wastes especially Municipal Solid Wastes and Refuse Derived Fuels.

Preprints (www.preprints.org) | NOT PEER-REVIEWED | Posted: 10 October 2023 doi:10.20944/preprints202310.0528.v1



**Table 2.** Methods for determination of kinetic parameters.

| Method | Equation | Reference |
|---|---|---|
| Friedman | $In\left[\beta\left(\frac{d\alpha}{dt}\right)\right] = -\left(\frac{E_\alpha}{R}\right)\left(\frac{1}{T}\right) + InAf(\alpha)$ | (Starink, 2003), (Fedunik-hofman et al., 2019) |
| Gupita | $In\left[\beta\left(\frac{d\alpha}{dt}\right)\right] = -\left(\frac{E_\alpha}{R}\right)\left(\frac{1}{T}\right) + InAf(\alpha)$ | (Gupta et al., 1988) |
| Freeman & Car-roll | $Y = -\frac{E}{R}X + n$<br>where, $Y = \frac{\Delta\, In\left(\frac{d\alpha}{dt}\right)}{\Delta\, In\,(1-\alpha)}$ and $X = \frac{\Delta\left(\frac{1}{T}\right)}{\Delta\, In\,(1-\alpha)}$ | (Jerez, 1983) |
| Kissinger-Akahira-Sanose (KAS) | $In\left(\frac{\beta}{T^2}\right) = -\left(\frac{Ea}{R}\right)\left(\frac{1}{T}\right) + In\left(\frac{A_\alpha R}{g_{(\alpha)}E_\alpha}\right)$ | (Danvirutai and Noisong, 2015) |
| Flyn-Wall-Onzawa (FWO) | $In\beta = -1.052\left(\frac{Ea}{R}\right)\left(\frac{1}{T}\right) + In\left(\frac{AE_a}{R\,g(\alpha)}\right) - 5.331$ | (Ozawa, 1965), (Joseph and Leo, 1966) |
| Starink | $In\left(\frac{\beta}{T^{1.95}}\right) = -\left(\frac{Ea}{R}\right)\left(\frac{1}{T}\right) + In\left(\frac{A_\alpha R}{g_{(\alpha)}E_\alpha}\right)$<br>$In\left(\frac{\beta}{T^{1.92}}\right) = -1.008\left(\frac{Ea}{R}\right)\left(\frac{1}{T}\right) + In\left(\frac{A_\alpha R}{g_{(\alpha)}E_\alpha}\right)$ | (Starink, 2003) |
| Boswel | $In\left(\frac{\beta}{T_{max}}\right) = -\left(\frac{Ea}{R}\right)\left(\frac{1}{T_{max}}\right) + constant$ | (Starink, 2003), (Boswell, 1980) |
| Coats and Redfern | $In\left(\frac{g(\alpha)}{T^2}\right) = -\left(\frac{Ea}{R}\right)\left(\frac{1}{T}\right) + In\left(\frac{AR}{\beta E}\right)$ | (Sajjad et al., 2017) |
| ASTM-E698 | $In\left[\beta\left(\frac{d\alpha}{dt}\right)\right] = -\left(\frac{E_\alpha}{R}\right)\left(\frac{1}{T}\right) + In[k_o(1-\alpha)]$ | (Osman et al., 2017) |
| Karaosmanoglu & Cif | $In\left[\frac{-1}{\alpha_o-\alpha_f}\frac{d\alpha}{dt}\right] = In(A) - \frac{E_a}{RT} + n\,In\left(\frac{\alpha-\alpha_f}{\alpha_o-\alpha_f}\right)$ | (Fernandez et al., 2017) |
| Isothermal method | $-In(t) = -\left(\frac{Ea}{R}\right)\left(\frac{1}{T}\right) + In\left[\frac{A}{g'(\alpha)}\right]$ | (Wang et al., 2014) |
| FWO and KAS Iterative methods | $In\left(\frac{\beta}{H_{(x)}}\right) = \left(\frac{0.0048A_\alpha E_\alpha}{g_{(\alpha)}R}\right) - \left(\frac{1.0516E_\alpha}{R}\right)\left(\frac{1}{T}\right)$<br>$In\left(\frac{\beta}{h_{(x)}T^2}\right) = In\left(\frac{A_\alpha R}{g_{(\alpha)}E_\alpha}\right) - \left(\frac{E_\alpha}{R}\right)\left(\frac{1}{T}\right)$<br>where<br>$H_{(x)} = \frac{(e^{-x})\,h_{(x)}/x^2}{0.0048\exp(-1.0516x)}$<br>and<br>$h_{(x)} = \frac{x^4+18x^3+86x^2+96x}{x^4+20x^3+120x^2+240x+120}$<br>which is the 4th degree Senum and Yang approximation that gives an accuracy better than $10^{-5}$ % for $x$ = E/RT ≥20. | (Senum and Yang, 1977), (Pérez-Maqueda and Criado, 2000) |
| Vyazovkin | $\Phi(E_\alpha) = \sum_{i=1}^{n} * \sum_{j\neq 1}^{n} \frac{J[E_\alpha, T_i(t_\alpha)]}{J[E_\alpha, T_j(t_\alpha)]}$<br>Where the time integral:<br>$J[E_\alpha, T_i(t_\alpha)] = \int_{t_{\alpha-\Delta\alpha}}^{t_\alpha} \exp\left[\frac{-E_\alpha}{RT_i(t)}\right] dt$<br>where, T(t) is the actual sample temperature, J is the integral with respect | (Vyazovkin and Wight, A, 1998), (Vyazovkin, 2006) |

Preprints (www.preprints.org) | NOT PEER-REVIEWED | Posted: 10 October 2023 doi:10.20944/preprints202310.0528.v1



| | | |
|---|---|---|
| | to T(t) and $T_i(t)$ is the temperature programs | |
| Kissinger | $In\left(\frac{\beta}{T_{max}^2}\right) = \left(-\frac{Ea}{R}\right)\left(\frac{1}{T_{max}}\right) + \frac{InAR}{Ea}$ | (Kissinger, 1956), (Blaine and Kissinger, 2012) |

In the equations (in table 2 above), α - is the fractional conversion, β - is the heating rate, A – is the pre-exponential factor, R – is the universal gas constant, and $E_a$ is the activation energy. The functions, g(α) – the integral form, and f(α) – the differential form, are used to determine the reaction mechanisms (Vyazovkin, 2006), (Vlaev et al., 2008) as shown in Table 3.

**Table 3.** Common mechanisms used during pyrolysis and degradation of solids.

| No. | Symbol | Name of the Function | *g(α)* | *f(α)* | Rate-determining mechanism |
|---|---|---|---|---|---|
| 1. Chemical process or mechanism non-invoking equations | | | | | |
| 1 | F1/3 | One-third order | $1-(1-\alpha)^{2/3}$ | $(3/2)(1-\alpha)^{1/3}$ | Chemical reaction |
| 2 | F3/4 | Three-quarters order | $1-(1-\alpha)^{1/4}$ | $4(1-\alpha)^{3/4}$ | Chemical reaction |
| 3 | F3/2 | one and a half order | $[(1-\alpha)^{-1/2}-1]$ | $2(1-\alpha)^{3/2}$ | Chemical reaction |
| 4 | F2 | Second order | $(1-\alpha)^{-1}-1$ | $(1-\alpha)^2$ | Chemical reaction |
| 5 | F3 | Third order | $(1-\alpha)^{-2}-1$ | $(1/2)(1-\alpha)^3$ | Chemical reaction |
| 2. Acceleratory rate equations | | | | | |
| 6 | P3/2 | Mampel power law | $\alpha^{3/2}$ | $(2/3)\alpha^{-1/2}$ | Nucleation |
| 7 | P1/2 | Mampel power law | $\alpha^{1/2}$ | $2\alpha^{1/2}$ | Nucleation |
| 8 | P1/3 | Mampel power law | $\alpha^{1/3}$ | $3\alpha^{2/3}$ | Nucleation |
| 9 | P1/4 | Mampel power law | $\alpha^{1/4}$ | $4\alpha^{3/4}$ | Nucleation |
| 10 | E1 | Exponential law | $ln\alpha$ | α | Nucleation |
| 3. Sigmoidal rate equations or random nucleation and subsequent growth | | | | | |
| 11 | A1, F1 | Avrami-Erofeev equation | $-\ln(1-\alpha)$ | $(1-\alpha)$ | Assumed random nucleation and its subsequent growth, n=1 |
| 12 | A3/2 | Avrami-Erofeev equation | $[-\ln(1-\alpha)]^{2/3}$ | $(3/2)(1-\alpha)[-In(1-\alpha)]^{1/3}$ | Assumed random nucleation and its subsequent growth, n=1.5 |
| 13 | A2 | Avrami-Erofeev equation | $[-\ln(1-\alpha)]^{1/2}$ | $2(1-\alpha)[-In(1-\alpha)]^{1/2}$ | Assumed random nucleation and its subsequent growth, n=2 |
| 14 | A3 | Avrami-Erofeev equation | $[-\ln(1-\alpha)]^{1/3}$ | $3(1-\alpha)[-In(1-\alpha)]^{2/3}$ | Assumed random nucleation and its subsequent growth, n=3 |
| 15 | A4 | Avrami-Erofeev equation | $[-\ln(1-\alpha)]^{1/4}$ | $4(1-\alpha)[-In(1-\alpha)]^{3/4}$ | Assumed random nucleation and its subsequent growth, n=4 |
| 16 | Au | Prout-Tomkins equation | $Ln[a/(1-\alpha)]$ | $\alpha(1-\alpha)$ | Branching nuclei |
| 4. Deceleratory rate equations | | | | | |
| 4.1 Phase boundary reactions | | | | | |
| 17 | R1, F0, P1 | Power law | α | $(1-\alpha)^0$ | Contracting disk |
| 18 | R2, F1/2 | Power law | $1-(1-\alpha)^{1/2}$ | $2(1-\alpha)^{1/2}$ | Contracting cylinder (Cylindrical symmetry) |
| 19 | R3, F2/3 | Power law | $1-(1-\alpha)^{1/3}$ | $3(1-\alpha)^{2/3}$ | Contracting sphere (spherical symmetry) |

Preprints (www.preprints.org) | NOT PEER-REVIEWED | Posted: 10 October 2023 doi:10.20944/preprints202310.0528.v1



| | | | | | |
|---|---|---|---|---|---|
| | 4.2 Based on the diffusion mechanism | | | | |
| 20 | D1 | Parabola low | $\alpha^2$ | $1/2\alpha$ | One-dimensional diffusion |
| 21 | D2 | Valensi equation | $\alpha+(1-\alpha)\ln(1-\alpha)$ | $[-\ln(1-\alpha)]^{-1}$ | Two-dimension diffusion |
| 22 | D3 | Jander equation | $[1-(1-\alpha)^{1/3}]^2$ | $(3/2)(1-\alpha)^{2/3}[1-(1-\alpha)^{1/3}]^{-1}$ | Three-dimensional diffusion, Spherical symmetry |
| 23 | D4 | Ginstling-Brounstein equation | $[1-2\alpha/3-(1-\alpha)^{2/3}$ | $(3/2)[(1-\alpha)^{-1/3}-1]^{-1}$ | Three-dimensional diffusion, Cylindrical symmetry |
| 44 | D5 | Zhuravlev, Lesokin, Tempelman equation | $[(1-\alpha)^{-1/3}-1]^2$ | $(3/2)(1-\alpha)^{4/3}[(1-\alpha)^{-1/3}-1]^{-1}$ | Three-dimensional diffusion |
| 25 | D6 | Anti-Jander equation | $[(1+\alpha)^{1/3}-1]^2$ | $(3/2)(1+\alpha)^{2/3}[(1+\alpha)^{1/3}-1]^{-1}$ | Three-dimensional diffusion |
| 26 | D7 | Anti-Ginstling-Brounstein equation | $1+2a/3-(1+a)^{2/3}$ | $(3/2)[(1+\alpha)^{-1/3}-1]^{-1}$ | Three-dimensional diffusion |
| 27 | D8 | Anti-Zhuravlev, Lesokin, Tempelman equation | $[(1+\alpha)^{-1/3}-1]^2$ | $(3/2)(1+\alpha^{4/3}[(1+\alpha)^{-1/3}-1]^{-1}$ | Three-dimensional diffusion |
| 5. Another Kinetic equation with unjustified mechanism | | | | | |
| 28 | G1 | | $1-(1-\alpha)^2$ | $½(1-\alpha)$ | |
| 29 | G2 | | $1-(1-\alpha)^3$ | $1/3(1-\alpha)^2$ | |
| 30 | G3 | | $1-(1-\alpha)^4$ | $1/4(1-\alpha)^3$ | |
| 31 | G4 | | $[-\ln(1-\alpha)^2$ | $(1/2)(1-\alpha)[1\ln(1-\alpha)]^{-1}$ | |
| 32 | G5 | | $[-\ln(1-\alpha)^3$ | $(1/3)(1-\alpha)[1\ln(1-\alpha)]^{-2}$ | |
| 33 | G6 | | $[-\ln(1-\alpha)^4$ | $(1/4)(1-\alpha)[1\ln(1-\alpha)]^{-3}$ | |
| 34 | G7 | | $[1-(1-\alpha)^{1/2}]^{1/2}$ | $4\{(1-\alpha)[1-(1-\alpha)^{1/2}\}^{1/2}$ | |
| 35 | G8 | | $[1-(1-\alpha)^{1/3}]^{1/2}$ | $6\{(1-\alpha)^{2/3}[1-(1-\alpha)^{1/3}\}^{1/2}$ | |

The thermodynamic parameters like entropy ΔS, pre-exponential factor (A), Gibbs free energy ΔG, and enthalpy ΔH (Sajjad et al., 2017) are determined as follows:

$$A = \beta . E_\alpha \, exp\left(\frac{E_\alpha}{RT_m}\right)/R.T_m^2$$

$$\Delta H = E_\alpha - RT$$

$$\Delta G = E_\alpha + R.T_m.In\left(\frac{K_b.T_m}{h.A}\right)$$

$$\Delta S = \frac{\Delta H - \Delta G}{T_m}$$

where $K_b$ is the Stefan Boltzman constant ($1.38*10^{-23}$ J/K), h is the Planks constant ($6.626*10^{-34}$ Js), and $T_m$ is the DTG peak temperature.

*3.3. Carbon monoxide from solid fuels: a persistent challenge*

Solid fuel emissions are dangerous to human health especially carbon monoxide (CO). It was observed that 5.2% of suicide deaths in England and Wales were due to CO poisoning in 2001-2011. These numbers declined to a total of 53 deaths by 2015 with England accounting for 91% of the total deaths (Office-for-National-Statistics-UK, 2016). Gas suicides cases reduced by 53% for the year between 2001 to 2011. However, there was a 17-fold increase fatal cases due to helium for the two-year period 2001-2002 to 2010-2011. Barbecue charcoal gas fatalities increased from one (1) to eleven (11) in the same period (Office-for-National-Statistics-UK, 2016), (Gunnell et al., 2015) Table 4.

Preprints (www.preprints.org) | NOT PEER-REVIEWED | Posted: 10 October 2023 doi:10.20944/preprints202310.0528.v1



**Table 4.** Number of deaths from accidental CO poisoning in England and Wales, deaths registered in 2011-20151,2,3. Adapted from the Office of National Statistics (UK) (Office-for-National-Statistics-UK, 2016).

| ICD 10 Code | Underlying cause | England | | | | | Wales | | | | |
|---|---|---|---|---|---|---|---|---|---|---|---|
| | | 2011 | 2012 | 2013 | 2014 | 2015 | 2011 | 2012 | 2013 | 2014 | 2015 |
| V00-X59 | All accidental carbon monoxide poisonings | 75 | 58 | 57 | 52 | 48 | 4 | 7 | 3 | 3 | 5 |
| X47 | Accidental poisoning by other gases and vapours | 33 | 23 | 22 | 25 | 24 | 1 | 2 | 2 | 1 | 1 |
| X47.0 | Occurrence at home | 28 | 17 | 14 | 18 | 23 | 1 | 1 | 2 | 0 | 1 |
| X47.1 | Occurrence in residential institution | 0 | 0 | 0 | 0 | 0 | 0 | 0 | 0 | 0 | 0 |
| X47.2 | Occurrence at school other institution/public admin area | 0 | 0 | 0 | 0 | 0 | 0 | 0 | 0 | 0 | 0 |
| X47.3 | Occurrence at sports/athletics area | 0 | 0 | 0 | 0 | 0 | 0 | 0 | 0 | 0 | 0 |
| X47.4 | Occurrence on street/highway | 1 | 1 | 0 | 0 | 0 | 0 | 0 | 0 | 0 | 0 |
| X47.5 | Occurrence at trade/service area | 1 | 0 | 0 | 1 | 0 | 0 | 0 | 0 | 0 | 0 |
| X47.6 | Occurrence at industrial/construction area | 0 | 0 | 1 | 0 | 0 | 0 | 0 | 0 | 0 | 0 |
| X47.7 | Occurrence on farm | 0 | 0 | 0 | 0 | 0 | 0 | 0 | 0 | 0 | 0 |
| X47.8 | Occurrence at other specified place | 3 | 4 | 6 | 4 | 1 | 0 | 1 | 0 | 1 | 0 |
| X47.9 | Occurrence at unspecified place | 0 | 1 | 1 | 2 | 0 | 0 | 0 | 0 | 0 | 0 |
| V01-V99 | Transport accident | 0 | 0 | 0 | 0 | 1 | 0 | 0 | 0 | 0 | 0 |
| X00-X09 | Accidental exposure to smoke, fire and flames | 42 | 35 | 34 | 27 | 23 | 3 | 5 | 1 | 2 | 4 |

[1] Cause of death was defined using the International Classification of Diseases, Tenth Revision (ICD 10). Deaths were selected where the underlying cause of death was accidental (ICD 10 codes V01-X59), and where the secondary cause of death was the toxic effect of carbon monoxide (ICD 10 code T58). The original underlying cause of death has been used. [2]Figures for England and Wales exclude deaths of non-residents based on boundaries as of November 2016. [3]Figures are for deaths registered, rather than deaths occurring in each calendar. Due to the length of time it takes to complete a coroner's inquest, it can take months or even years for a carbon monoxide poisoning death to be registered. More details can be found on the ONS website: www.ons.gov.uk/ons/guide-method/user-guidance/health-and-life-events/impact-of-registration-delays-on-mortality-statistics/index.html.

The Gas Safety Trust (GST) of the UK has also been compiling statistics on CO related death by fuel type (CO-Gas-Safety, 2015a) as well as other accidental death and injuries (Gas Safety Trust - UK, 2017), (CO-Gas-Safety, 2015b) especially from 1995 to date (Gas Safety Trust - UK, 2019), (Gas Safety Trust - UK, 2018).

## 4. Systems for minimising CO released from solid fuels

There are various approaches used to minimize the CO emissions from solid fuel combustion, each of which is designed depending on the specific application. The main approaches include cooking systems, heating systems, catalytic systems, and sensors/detectors Figure 5. Some applications employ a combination of two or more depending on the complexity and desired outcomes.

Preprints (www.preprints.org) | NOT PEER-REVIEWED | Posted: 10 October 2023 doi:10.20944/preprints202310.0528.v1



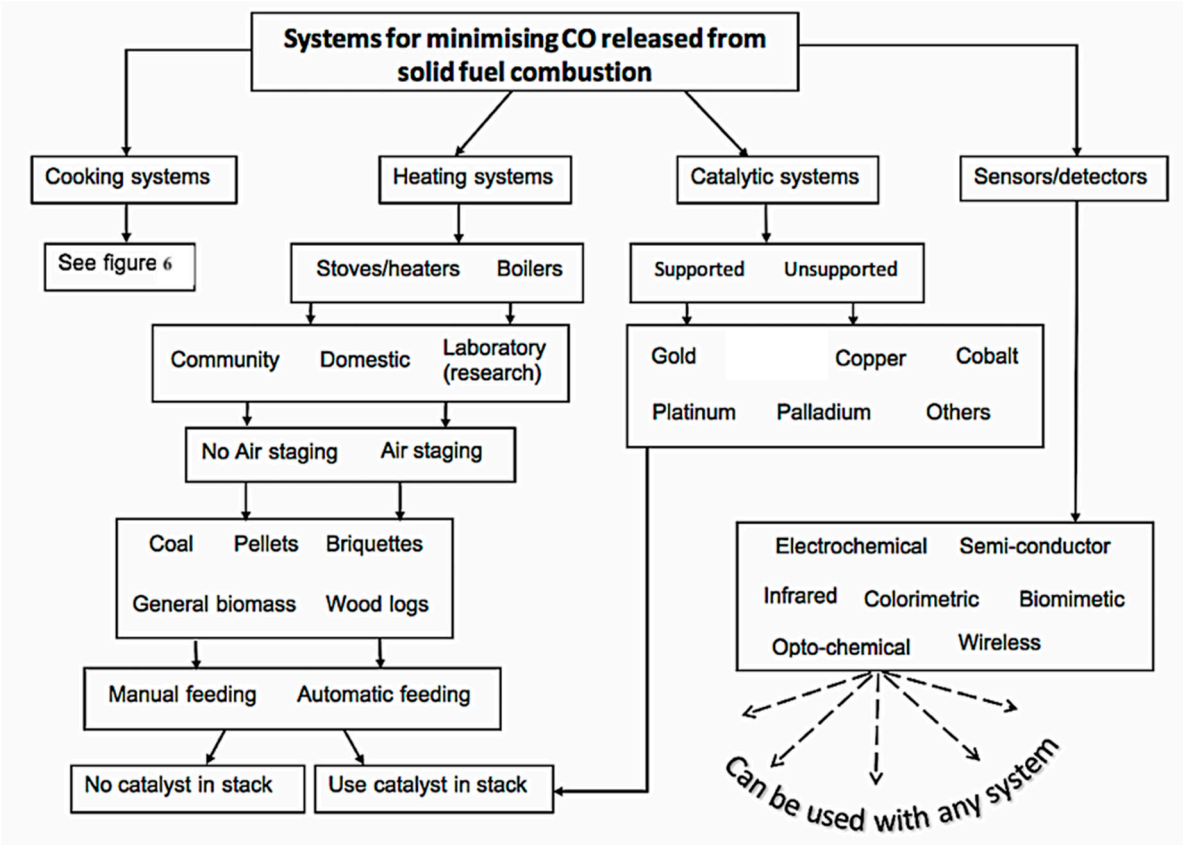


**Figure 5.** Systems for minimising CO from solid fuel combustion.

*4.1. Improved cookstoves*

Cooking on traditional cookstoves or three stone open fires has been reported as being inefficient in terms of energy as well as emission reduction of combustion pollutants. Technologically advanced/improved cookstoves (Jetter et al., 2012) (including Phillips cookstoves (Coffey et al., 2017), small scale gasifier cooking stove (MacCarty et al., 2010), (Njenga et al., 2016), (Njenga et al., 2017), stoves with electrical fans and chimneys (Still et al., 2015), rocket-type stoves, pot skirt stoves (MacCarty et al., 2010) among others) emitted less CO and other combustion pollutants and were more fuel-efficient than traditional stoves. However, the amounts of particulate matter are not much reduced (for Phillips cookstoves) (Coffey et al., 2017). Charcoal burning stoves (Still et al., 2015) were better than batch fed stove by up to 40% thermal efficiency. The daily carbon emissions from charcoal stoves in Kenya (Bailis et al., 2003) were lower than both traditional open fire and improved ceramic woodstoves. However, when each pollutant was weighted using a 20-yr global warming potential, charcoal stoves emitted larger amounts of greenhouse gases than a woodstove, open fire and ceramic woodstoves. Even the non-$CO_2$ emissions from charcoal stoves were higher for the 20-yr equivalent units compared to the three-stone fires and improved ceramic stoves. The combustion transition from wood to charcoal reduces PM emissions by 87% during the burning period and by 92% during smoldering when using ceramic wood-burning stoves compared to traditional cookstoves (Ezzati et al., 2000). Using accessories for pre-ignition may also save energy and minimise emissions. Using a lighting cone (Lask and Gadgil, 2017) as an accessory to shallow-bed charcoal stoves, ignition time, fuel (charcoal) consumption, and CO emissions were reduced by up to 50%, 40%, and 50% respectively. Improved cookstoves are durable and usually manufactured with locally available raw materials (Mehetre et al., 2017). The various classifications of traditional and improved cookstoves are shown in Figure 6.

Preprints (www.preprints.org) | NOT PEER-REVIEWED | Posted: 10 October 2023 doi:10.20944/preprints202310.0528.v1



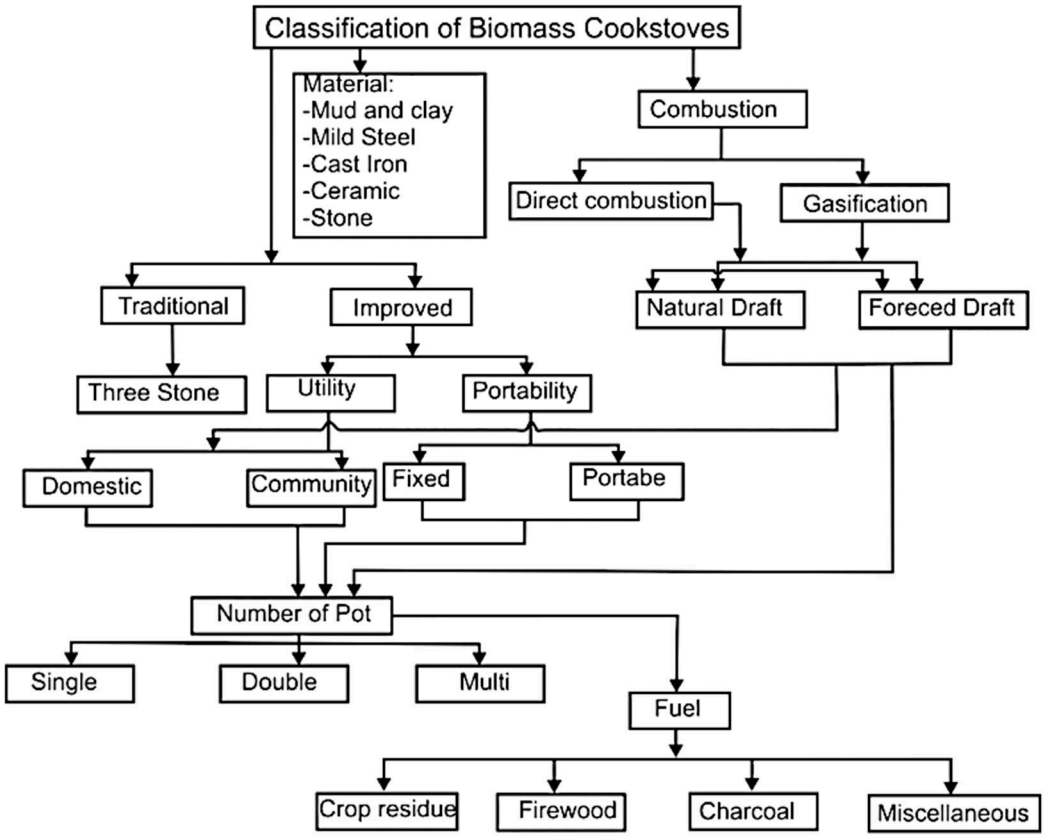


**Figure 6.** Classification of biomass cookstoves *(Mehetre et al., 2017).*

Some stoves are constructed with a layer of catalyst to enhance CO oxidation. However, the addition of $K_2Ti_2O_5$ to the monolith reduced CO emissions compared to the blank monolith but was unable to reduce CO emissions to the level of a stove without a catalyst *Figure 7*. The thermal efficiency of all the tested stove configurations were equally the same at about 25% for both low and high power operation (Paulsen et al., 2018). The different relevant research published on improved cookstoves is shown in Table 5.

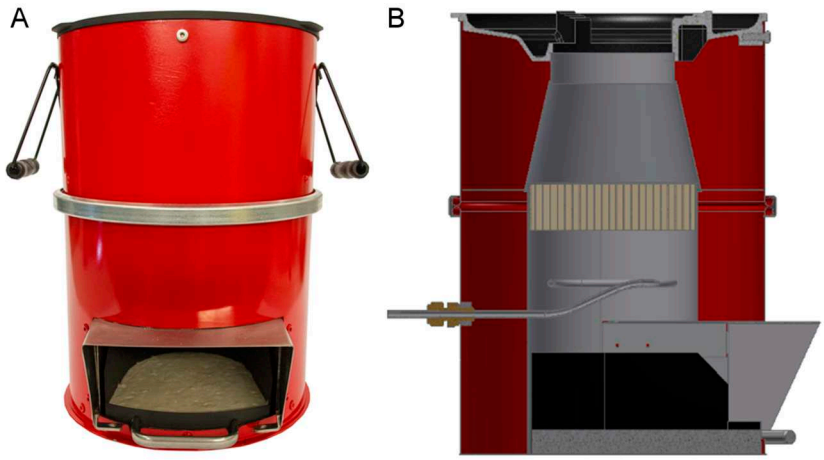


**Figure 7.** Rocket stove used for catalyst testing. (A) Picture of the rocket stove used during testing and (B) diagram of the rocket stove showing the catalytic monolith placement (Paulsen et al., 2018).

Preprints (www.preprints.org) | NOT PEER-REVIEWED | Posted: 10 October 2023 doi:10.20944/preprints202310.0528.v1



**Table 5.** Descriptions of the various improvements made on traditional cook stoves.

| Description of traditional stoves | Description of improved stoves | CO from traditional stove | CO from improved stove | % CO reduction | Reference |
|---|---|---|---|---|---|
| Three-brick stove, a cooking pot placed over the bricks uses fire wood | Made of clay and husk, two cooking pots, and a stack | 10 ppm | 2.5 ppm | 75 | (Jamali et al., 2017) |
| | stoves with chimneys or smoke hoods | 11.9 ppm[a] | 5.1 ppm[b] | 57.1 | (Pope et al., 2017) |
| | stoves without chimneys or smoke hoods | 10.8 ppm[a] | 6.6 ppm[b] | 38.7 | (Pope et al., 2017) |
| | Charcoal stoves | 27.4 ppm[a] | 9.6 ppm[b] | 64.9 | (Pope et al., 2017) |
| | Advanced combustion stoves | 11.3 ppm[a] | 5.7 ppm[b] | 49.7 | (Pope et al., 2017) |
| The Hifadhi stove has an air entrance and a combustion chamber. | Galvanised Gasifier cook stove | 42 ppm | 20 ppm | 52.0 | (Njenga et al., 2016) |
| Three stone cook stove - burning prunings, maize cobs, and coconut shells | Galvanised Gasifier cook stove | 36.5 ppm | 20 ppm | 45 | (Njenga et al., 2016) |
| Three-stone open fires for burning wood | Metal braziers for burning charcoal | 19.4 ppm | 7.6 ppm | 60.8 | (Tagle et al., 2018) |
| Open in the home, or in an annexed kitchen or outside the home, or under a ledge along outer house wall | Stove with chimney, in good condition; little to no visible damage | 5.0% | 4.6 % | 8.0 | (Lucarelli et al., 2018) |
| Open fire or poorly designed combustion chambers– burning wood | Improved stove: with a chimney and a better combustion system – burning wood | 14.3 ppm | 1.8 ppm | 87.4 | (Clark et al., 2009) |
| The traditional stationary hearth and the portable hearth. All burn biomass | Philips advanced biomass combustion stoves, with two-stage combustion & forced air | 30 ppm | 7.4 ppm | 75.3 | (Mukhopadhyay et al., 2012) |
| Traditional three-stone open fires for burning wood | Envirofit B1200-Natural Draft (rocket stove) | 9.6 ppm | 6.4 ppm | 33.3 | (Sambandam et al., 2015) |
| | Envirofit G3300 Natural Draft rocket stove | 10.2 ppm | 7.5 ppm | 26.5 | (Sambandam et al., 2015) |
| | Prakti Leo-Natural Draft (rocket stove) | 11.6 ppm | 4.7 ppm | 59.5 | (Sambandam et al., 2015) |
| | Philips-Natural Draft (micro gasifier) | 3.6 ppm | 3.2 ppm | 11.1 | (Sambandam et al., 2015) |
| | Philips-Forced Draft (micro gasifier) | 29 ppm | 9.6 ppm | 66.9 | (Sambandam et al., 2015) |

Preprints (www.preprints.org) | NOT PEER-REVIEWED | Posted: 10 October 2023 doi:10.20944/preprints202310.0528.v1



| | | | | | |
|---|---|---|---|---|---|
| Traditional 3 stone | Oorja forced draft micro gasifier using pellets | 4.3 ppm | 2.7 ppm | 37.2 | (Sambandam et al., 2015) |
| | Eco Chula - Electric fan-assisted gasifier | 6.5 ppm | 5.4 ppm | 16.9 | (Yip et al., 2017) |
| | EcoZoom - Improved rocket | 6.5 ppm | 6.7 ppm | -3.1 | (Yip et al., 2017) |
| | Envirofit - Improved rocket | 6.5 ppm | 4.9 ppm | 24.6 | (Yip et al., 2017) |
| | Philips - Electric fan-assisted gasifier | 6.5 ppm | 3.8 ppm | 40.0 | (Yip et al., 2017) |
| | Prakti - Double pot rocket with chimney | 6.5 ppm | 4.5 ppm | 30.8 | (Yip et al., 2017) |
| | Built-in rocket stove | 6.5 ppm | 4.4 ppm | 32.3 | (Yip et al., 2017) |

[a]Before intervention. [b]After intervention. Interventions to reduce exposure to household air pollution can be classified broadly as (i) those acting to change the primary household fuel, (ii) those promoting cleaner-burning and more efficient solid fuel stoves, (iii) those improving the living environment and (iv) those modifying user behaviour.

In India, (Ministry of New and Renewable Energy - India, 2015) approving stove designs was based on their performance as per BIS 13152(part 1) 2013 specification. These include domestic size stoves with natural draft operation having a thermal efficiency in the range 25 – 33.57 % and CO emissions in the range 2.50 – 4.64 g/MJ. Similarly, domestic size cookstoves with forced draft systems had a thermal efficiency range of 35.3 – 40.90 % and CO emission range of 1.12 – 3.2 g/MJ. Community size stoves with natural draft were also approved having a thermal efficiency of 28.1 – 30.28 % and CO emission range of 1.15 – 1.73 g/MJ. Forced draft community stoves, on the other hand, had a thermal efficiency of 35.11 – 42.8 % and CO emission range of 0.83 – 1.97 g/MJ.

### *4.2. Heating systems*

#### 4.2.1. Air staging/two-stage combustion

Air staging or two-stage combustion is the introduction of overfire air into the furnace. During the furnace overfire air technology, combustion air is injected into the system that separates it into primary and secondary flow sections. The aim is to convert all the CO to $CO_2$. About 70-90% of the primary air is introduced into the fuel to produce an oxygen-rich, low temperature, fuel-rich zone which minimizes the amount of CO formed. On the other hand, 10-30% of secondary air is injected through nozzles above the combustion area in a special wind-box. This increased flow volume completes the combustion process. Figure 8, shows a representation of a modern and a traditional masonry heater employing air staging.

Preprints (www.preprints.org) | NOT PEER-REVIEWED | Posted: 10 October 2023 doi:10.20944/preprints202310.0528.v1



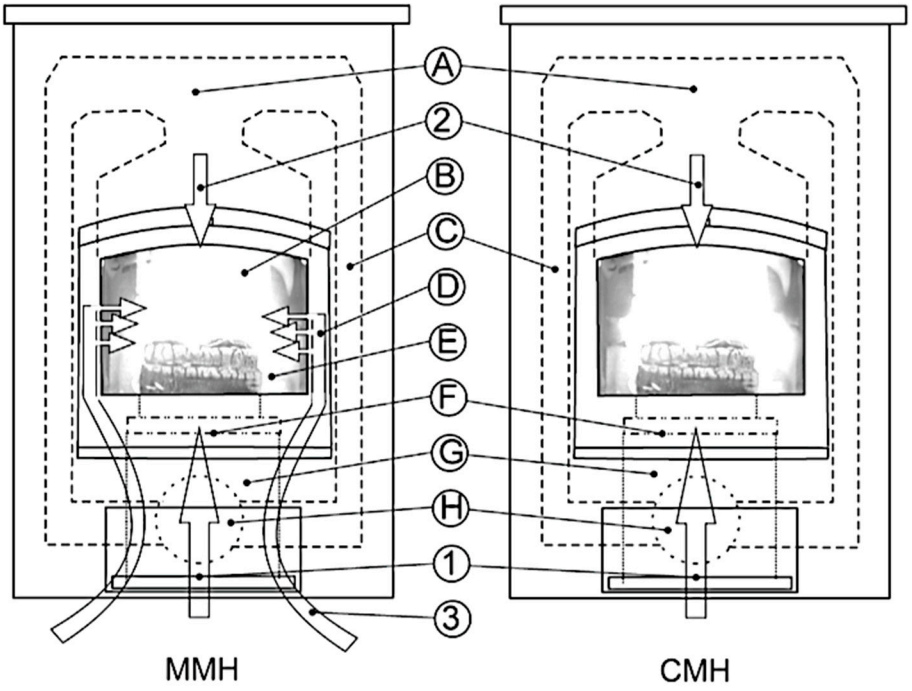


**Figure 8.** Representation of a Modern (MMH) and Conventional Masonry Heater (CMH). 1, Primary air supply; 2, Window flushing air supply; 3, Secondary air supply; A, Upper combustion chamber; B, Secondary combustion zone; C, Flue gas ducts; D, Secondary air flow between ceramic plates; E, Primary combustion zone; F, Rift grate; G, Ash box; H, Flue gas exhaust to chimney (behind the heater) (Nuutinen et al., 2014).

With air staging, the samples for analysis of emissions are collected from the flue gases arising from the combustion system/boiler outlet/stack of the boiler. In 2002, a 30 kW boiler (Ross et al., 2002) with a ceramic chimney-stack fitted with temperature and pressure sensors to burn Polish bituminous coal, Lump wood pine, Pine sawdust briquettes, and Coal + sawdust briquettes. They used on-line flue gas monitoring using IR analysis for CO analysis. They observed that lump wood produced a higher total organic content, methane and CO emission than biomass briquettes. Laboratory wood pellet boiler (25-kW) have also been studied (Lamberg et al., 2011), measuring emissions with ABB Cemas gas-analyzing rack system. Their system produced CO emissions as low as 3.55 mg/MJ and as high as 335 mg/MJ. A similar laboratory masonry heater burning birch wood and CO detection with ABB Cemas Gas Analyzing Rack & FTIR were used (Nuutinen et al., 2014) in 2014. A CO reduction in the range of 26 to 81% was achieved.

A slightly stronger 35 kW ETA Hack35 tilting grate biomass boiler was used a year after (Carroll et al., 2015) burning wood, willow, and cocksfoot. They used a portable gas analyser with NDIR for CO analysis and achieved low CO emissions of 18 mg/Nm$^3$ at a primary split ratio of 1.6. In 2016, a 5–12 kW low-scale combustor (Combustor, 2016) with air staging was analysed while burning biomass and measuring CO with a servomex gas analyser. They observed that CO emissions were in the range of 0.2 – 0.6 % with 6% oxygen and air excess of 1.4 – 2.0. A year later, laboratory-scale reactor (Khodaei et al., 2017), burning standard cylindrical wood pellets were used to simulate CO reduction strategies. Emissions were analysed with Servopro 4900. They observed that CO was in the range of 0.1–0.5%.

In the same year (2017), (Sher et al., 2017), a 20 kW bubbling fluidised bed combustor burning domestic & industrial wood, miscanthus, straw, and peanut shell pellets was investigated. They measured CO with ABB, EL3020 analyser and observed only 0.1 – 0.6 vol% as CO emissions. Still, in 2017, a hybrid stove burning biomass was able to reduce CO emissions by 65% (Lamberg et al., 2017). In 2018, a 140-kW fixed bed biomass boiler (Caposciutti and Antonelli, 2018) was used for burning biomass and they observed that low CO emissions were obtained for the split ratio of 0.4 and air

 doi:10.20944/preprints202310.0528.v1



excess of 1.5 –2.5. In the same year, an OP 230 boiler - two-pass drum boiler burning pulverized hard coal was used to investigate an air-staging system (Hernik et al., 2018). They observed that low CO emissions were achieved where overfire air was perpendicular to the surface of the nozzles.

4.2.2. Improved boiler systems

The improved boilers work by reducing incomplete combustions through the optimization of the combustion system due to the improvement of boiler efficiency and CO emissions reduction by boiler manufacturers with or without the automatic airflow control system. They may have continuous or periodic feeding operations (Johansson et al., 2004). The materials used for such boiler systems range from sewage sludge, coffee husks, wheat straw, briquettes made from; corn stover, rye straw, miscanthus, cherry stones, cylindrical briquettes, hay and sunflower husk pellets, pellets mixture (deciduous and coniferous wood). The feedstock could also be basket willow-chips, rape straw-briquettes, Wood waste-pellets, Poplar firewood-chips, Sawdust, Oak bark shavings, from a sawmill, Rape cake, coal. Wood pellets, wood briquettes, wood logs and oil, grain whole crop (triticale), hay, and forest residue wood could also be used. The woods could be of particle length of 1 to 2 cm, while the herbaceous fuels could be as both, pellets (12 mm diameter, 25 mm mean length) and chopped material (20 mm mean copping length).

In the year 2000, a 15 and 50 kW modern multi-fuel furnace (Launhardt and Thoma, 2000) that burnt biomass and wood pellets were investigated for their effectiveness in reducing CO emissions. They observed that CO-emissions were all around 200 mg/m$^3$; related to the fuel type. Four years later, CO emissions from Old-type wood boilers (6-24 kW), Modern wood boilers (12-34 kW), Pellet burners (3-11 kW), and Oil burners (18-21 kW) (Johansson et al., 2004) were also analysed. They observed that long residence time, high temperature and adequate mixing of air & combustible gases reduced CO emissions.

Using a 50 kW Arimax 340 fixed retort system biomass boiler (Bignal et al., 2008), the full flame boiler conditions had low CO while the slumber mode had high CO emissions. Figure 9, shows the relationship between the total PAHs and CO emissions for the different boiler operating conditions. A year later (Ozil et al., 2009), two 13 kW domestic wood heating fireplaces with catalyst systems: cordierite honeycomb monolith and metallic corrugated structure in their chimney were investigated. They observed that a switch of normal to low-charge phase increased CO emissions. Having a catalyst in the chimney reduced CO emission by up to 80% at ignition and to 90% in the low-charge phase. In 201, a 6 kW pellet stove; a 40 kW biomass boiler; a 6.5 kW simple logwood stove and a 6 kW logwood stove (Schmidl et al., 2011), were investigated for their effectiveness in minimising CO emissions. It was observed that full load conditions in automatically fired systems exhibited very low CO emissions compared to manually fired systems.

Preprints (www.preprints.org) | NOT PEER-REVIEWED | Posted: 10 October 2023 doi:10.20944/preprints202310.0528.v1



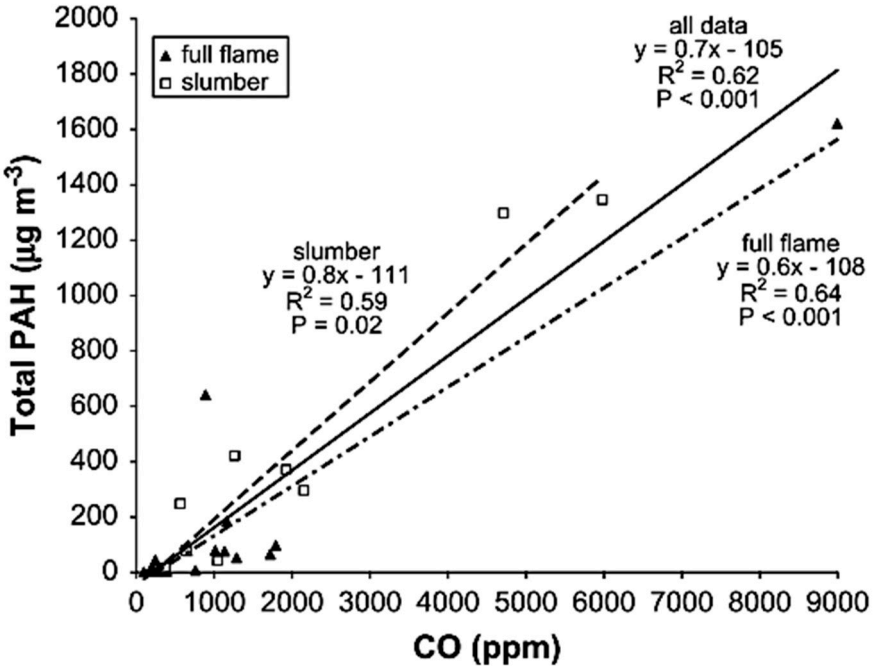


**Figure 9.** Release of polycyclic aromatic hydrocarbons, carbon monoxide and particulate matter from biomass combustion in a wood-fired boiler under varying boiler conditions *(Bignal et al., 2008)*.

A year later (2012), a 15-kW horizontal-feed furnace (Juszczak and Lossy, 2012), was investigated having been installed in a down-draft wood log boiler. They observed that the higher the proportion of wood pellets in the mixture the lesser slag and the lower CO in the flue gas. In the same year, a vertical laboratory-scale furnace (Jeguirim et al., 2012) that burnt date palm residues was used for CO investigations. They used a Rosemont IR analyzer for CO analysis. It was observed that secondary air supply and proper air mixing reduced CO emissions. Again in 2012, the use of a 20 kW wood pellet boiler, and a pellet stove combined (Win et al., 2012) with a solar heated buffer store were analysed. They observed that the pellet stove with efficient air staged combustion produced the lowest CO.

In 2013, (Rabaçal et al., 2013), observed that a 22 kW domestic wood pellet-fired boiler could reduce CO emissions if operated at high temperature and high air excess. Juszczac (Juszczak, 2014), in 2014 observed that a 25 kW water boiler equipped with an over-fed wood pellet furnace conditions burning ECOPELLET wood pellets reduced CO emissions as oxygen in the system was increased. In the same year, (Win and Persson, 2014), using a 12, 20, and 25-kW wood pellet boilers and a pellet stove of the nominal power of 12 kW observed that the CO emissions increased with decreasing combustion power.

In 2015, (Calvo et al., 2015) used a manually operated wood stove with handheld control of combustion air, and a traditional Portuguese brick open fireplace to investigate toxic combustion emissions. They observed that CO emissions from the fireplace were higher than those observed for the stove. The following year, (Juszczak et al., 2016) investigated a 20-kW full-scale heat station connected with district heating network burning biomass pellets and Coal for emission control. They observed that increased temperatures and oxygen availability reduced CO emissions. Again in 2016, (Tschamber et al., 2016) performed experiments with an airtight cast-iron stove that burnt wood logs. Low CO emissions were recorded with the airtight cast-iron stove in comparison to other stoves and fireplaces of the 1990s or new ones without post-combustion system. In the same year, (Mantananont and Patumsawad, 2016) used a lab-scale fixed-bed combustion system burning Thai lignite and agricultural residues, rice husk, rice straw, and bagasse to investigate the toxic combustion emissions. They observed that CO emissions reduced considerably as secondary air/total air ratio was increased.

 doi:10.20944/preprints202310.0528.v1



In 2017, (Zajac et al., 2017) investigated a 32-kW boiler with automatic fuel load burning wood pellets with UL- TRAMA T 23 analyser for emission analysis. They observed that temperature and fuel type influenced CO emissions. In the same year, (Wielgosi!nski et al., 2017) used an electric resistance furnace and a pipe furnace with a horizontal working chamber to analyse emission reduction effectiveness. They found out that increasing aeration decreased the amount of CO, especially at elevated temperatures. More recently, (Byul et al., 2018) used a 3.0 MW KFS subsidized industrial wood pellet boiler to monitor emission reduction for 3 years. They observed that the system was able to achieve a 58.9 % CO reduction between 2012 to 2015. In the same year, (Pałaszynska and Juszczak, 2018) used a 50 kW boiler type Bio-warmer that burnt sewage sludge, coffee husks, wheat straw, biomass briquettes, and miscanthus to investigate combustion emissions. They observed that except for sewage sludge pellets, CO did not exceed 3000 mg/m$^3$.

The main challenges facing cooking and heating systems are variation in fuel quality and proper mixing to optimize the available air for enhanced oxidation. Feedstocks are obtained from different locations and their growth patterns, soil conditions, nutrient availability and climate dictate the final quality (moisture content, volatiles, fixed carbon, mineral content, among others). Applying different recipes like single biomass species batches, mixed biomass, co-firing, single coal batches, mixed coal batches have all been applied to solve this challenge. With optimizing air mixing, self-adjusting controls that use sensors have been used for CO, temperature and air-excess (Nussbaumer, 2003). But still, the mixing of combustibles with air is a challenge. The application of computational fluid dynamics for extended simulation and modelling is being used to solve the mixing challenge.

### *4.3. Catalytic oxidation of CO*

#### 4.3.1. Carbon monoxide and oxygen chemisorption on metals

Carbon monoxide

The adsorption and reactivity of carbon monoxide on oxides and metals is a result of CO having three resonance structures. By donating electrons through the 5s orbital and accepting electrons through the antibonding 2p* orbital makes it possible for carbon monoxide to be coordinated to one or numerous species. Five spectral ranges of CO adsorption bands can be detected depending on the number species it is bonded to 1700–1800, 1800–1920, 1860–2000, 2000–2130, and 2130–2200 cm-1. The particle size and the nature of the metal site will determine the IR band position. Platinum, rhodium, and palladium have been used to oxidise CO and have given infrared vibration bands at different positions depending on the orientations (mirror indices) of these metals. Chemisorption behavior of carbon monoxide on metals also varies considerably: for Pt, Rh, and Ru, the heat of chemisorption is directly proportional to the metal surface density. Also, the heats of chemisorption are inversely proportional to CO coverage ($q$CO) with platinum having the highest sensitivity (Royer and Duprez, 2011).

Oxygen

For CO oxidation to be fully understood, the chemisorption of oxygen on catalyst surfaces must be understood as well. Unlike CO, adsorption of oxygen is dissociative. The heat of adsorption on most non-noble transition metals is mostly not affected by oxygen coverages. However, noble metals (Rh, Pd, Pt) have inverse relations of the heat of chemisorption with oxygen coverage. This is due to differences in the metallic radius of the metals Figure 10.

Preprints (www.preprints.org) | NOT PEER-REVIEWED | Posted: 10 October 2023 doi:10.20944/preprints202310.0528.v1



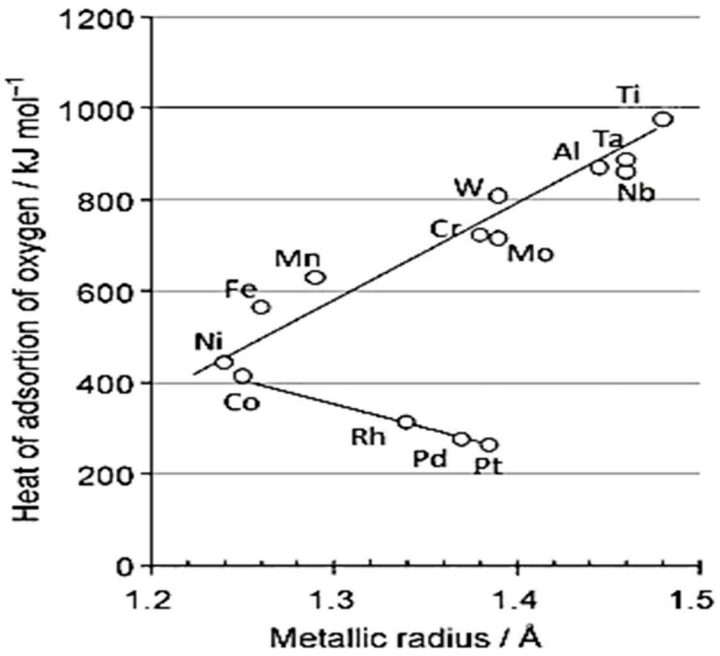


**Figure 10.** Heat of adsorption values of metals, as a function of their metallic radius. Adapted from (Royer and Duprez, 2011).

4.3.2. Laboratory oxidation of CO over metals

Supported metal catalysts

The presence of catalyst support may have a significant effect on the catalyst activity and the overall reaction. The final reaction usually occurs on the catalyst or at the catalyst/support interface. Secondly, the oxidation/reduction state of the metal catalyst has a major implication on CO oxidation (Royer and Duprez, 2011).

CO oxidation over simple oxide catalysts

Much as noble metals are very active for oxidation of CO, some oxides especially Cu and Co have shown remarkable activity as well for CO oxidation. The reactivity of noble metals and base metal oxides for oxidation of 1% CO in excess oxygen and 300 $^{o}$C follows the order; Pd > Pt > $Co_2O_3$ > CuO > $CuO/Cr_2O_3$ > $LaCoO_3$ > Au > $MnO_2$ > $Fe_2O_3$ > $Cr_2O_3$ > NiO (Royer and Duprez, 2011).

Gold-based catalysts

The ability to change oxidation states by gold and ceria has played a great role during the catalytic oxidation of carbon monoxide (R. Zhang et al., 2017). This is also due to their oxygen vacancies, and high oxygen storage capacity of this catalyst system. The shape of ceria as support also influences the catalytic activity of gold for CO oxidation. Carltonbird *et al*. (Carltonbird et al., 2018), observed that the order of reactivity of gold catalyst in relation to the shape of ceria support was; rod-shaped > polyhedral > cube > octahedral shaped $CeO_2$. However, the addition of iron to the $Au/CeO_2$ system improved the catalytic activity for oxidation of CO and benzylamine compared to $Au/CeO_2$ alone (Sudarsanam et al., 2014). A gold/titania-based catalyst is a unique combination in that on top of achieving 100% conversion of CO at room temperature, it displayed remarkable CO oxidation at 120 K (Lee and Zaera, 2014). Other researchers have reported a gold catalyst supported on various supports for the oxidation of CO and alcohols. Such systems included Au/activated carbon, Au/boron nitride, Au/titanium dioxide, and Au/mesoporous silicate-based (SBA-15) (Song et al., 2017). Perovskites ($LaMnO_3$, $LaFeO_3$, $LaCoO_3$, and $LaCuO_3$) have also worked excellently as

 doi:10.20944/preprints202310.0528.v1



supports for gold. With only 1wt% of gold, superior activity was registered for CO oxidation (Mokoena et al., 2016). Gold supported on three dimensional $Mn_2O_3$ was used for CO, and toluene oxidation (Xie et al., 2014). At only 15 $^oC$, up to 90% conversion was achieved. This was attributed to its low-temperature reducibility, high oxygen adsorption capability, high porosity and the strong interaction between gold nanoparticles and the three-dimensional $Mn_2O_3$. In other studies, a gold-copper alloy supported on MgO or graphene (Koizumi et al., 2015) has been used for efficient oxidation of CO. This combination was preferred for its effectiveness and commercial affordability compared to other gold-based catalysts.

Copper-based catalysts

Water-resistant SnCu30 (30wt%Cu) catalysts have been prepared and used for oxidation of CO (Bai et al., 2017). The high activity was attributed to the lattice surface oxygen and the highly dispersed $Cu^+$ species within the Cu-$SnO_2$ catalyst matrix which provided active sites for adsorption of CO. Un-supported CuO uses the surface area advantage for oxidation of CO. A decrease in specific surface area of CuO from 90 to 8 $m^2/g$ resulted in a four-fold increase in the specific catalytic rate (Svintsitskiy et al., 2016). However, a 20-fold decrease in the specific catalytic rate was observed when the catalyst specific surfaces area was reduced to 1 $m^2/g$. Activated-red-mud as support on CuO produces a well-structured porous and high surface area catalyst (Hu et al., 2016) for CO oxidation. However, the CO oxidation is dependent on CuO loading and the catalyst calcination temperature. Copper-Manganese (commercially known as hopcalite) prepared by flame spray pyrolysis produced a superior hydrophobic catalyst that was resistant to humidity levels as high as 75% (Biemelt et al., 2016). This was achieved by applying 2-ethyl hexanoate as precursors achieving a high specific surface area catalyst (180 $m^2/g$) composed of $Cu_{1.5}Mn_{1.5}O_4$ as the main phase. A more sophisticated Cu-based catalyst composed of Cu-Pd/$CeO_2$ (Du et al., 2017) achieved excellent activity for CO oxidation. This was attributed to full oxidation of the Cu and Pd by the ceria support which dominated the catalyst system providing an excellent metal/support interaction.

Cobalt catalysts

The catalyst preparation method greatly impacts its performance. Dispersion–precipitation synthesis of $Co_3O_4$ produced a better catalyst for oxidation of carbon monoxide and propane than alkali-induced precipitation (W. Zhang et al., 2017). Dispersion–precipitation produced a more reducible $Co_3O_4$ catalyst with high numbers of active surface oxygen species. The activation energy for CO and C3H8 oxidation were reduced by 38% and 31% respectively with the dispersion–precipitation synthesised $Co_3O_4$ compared to alkali-induced precipitation synthesised $Co_3O_4$. Titania supported $Co_3O_4$ catalyst prepared by incipient wetness impregnation had a superior activity for CO and hydrocarbon oxidation in vehicle exhaust emissions compared to $Co_3O_4/TiO_2$ catalyst prepared by wet impregnation method (W. Ahmad et al., 2017). Similarly, the activity of hollow type $Co_3O_4$ spheres prepared using silica templates for CO oxidation was dependent on calcination temperature with 623 K producing the best activity (Umegaki et al., 2016). These hollow sphere $Co_3O_4$ catalyst also showed superior activity compared to supported $Co_3O_4$ as well as $Co_3O_4$ nanoparticles. In a similar situation, Cao *et al.* (Cao et al., 2014) observed that the wormhole-like-mesoporous Co-Fe-O catalyst activity for CO oxidation was dependent on Co loading (Figure 11), the surface area, the pre-calcination temperature, and the particle size.

Preprints (www.preprints.org) | NOT PEER-REVIEWED | Posted: 10 October 2023 doi:10.20944/preprints202310.0528.v1



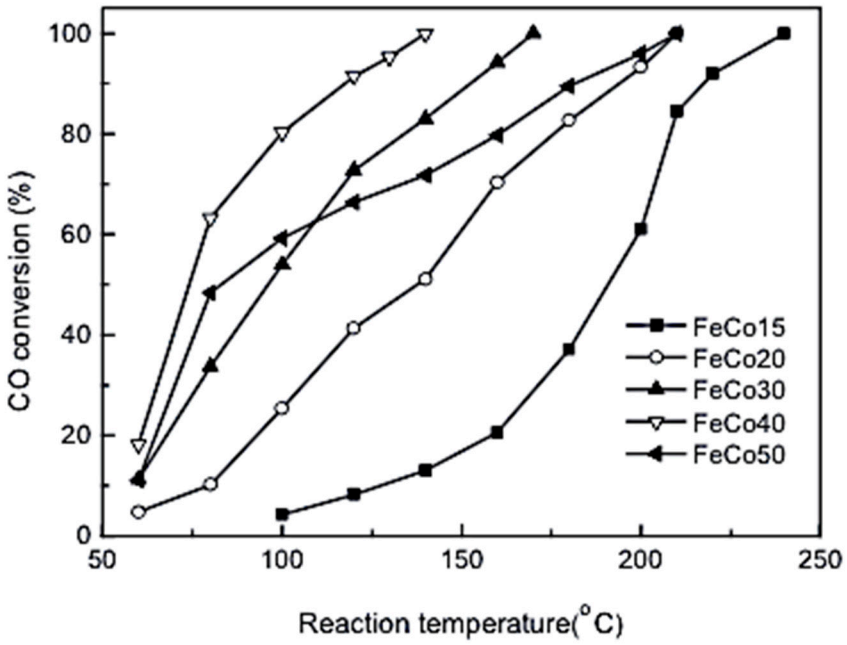


**Figure 11.** Mesoporous Co-Fe-O nanocatalysts: Preparation, characterization and catalytic carbon monoxide oxidation *(Cao et al., 2014)*.

Platinum and Palladium catalysts

Being noble metals, a small concentration is needed in addition to a support for efficient CO catalytic activity. With only 0.5wt%Pd/manganese oxide catalyst, maximum CO, toluene, and ethyl acetate oxidation were achieved at 55°C compared to un-supported Pd catalyst. This excellent activity was attributed to high oxygen adsorption and low-temperature reducibility of the 0.5wt%Pd/manganese oxide catalyst. With $LaMnO_3$ Perovskites, palladium loading was directly proportional to CO catalytic activity (Kucharczyk, 2015). The activity was seen to increase with the temperature especially in the range 650 to 800 °C.

$Pt/CeO_2$ catalysts prepared by impregnation-reduction (Hong and Sun, 2016) had the best activity for complete oxidation of CO at room temperature compared to the same catalyst prepared by impregnation, and deposition-precipitation methods. The activity of the impregnation-reduction prepared $Pt/CeO_2$ catalyst was attributed to possessing highly numbers of negative Pt species for efficient adsorption of oxygen for CO oxidation. Similarly, acid treatment followed by thermal activation of palladium–copper complexes affected the catalyst's activity for CO oxidation (Rakitskaya et al., 2016). The best results were obtained when the bimetallic Pd(II)–Cu(II) complexes were treated with 3M $HNO_3$ for 0.5 and heat-treated for 60 minutes.

Ceria based catalysts

Ceria being a base metal oxide works better with a support and at intermediate temperatures. It was reported that ceria/alumina could achieve complete oxidation of 7739 ppm of CO at 400 °C in excess oxygen compared to un-supported ceria (Wilklow-Marnell and Jones, 2017). Similarly, a ceria-zirconium catalyst system doped with low amounts of Nd (<0.1wt%) was reported to enhance the surface area of the catalyst thereby improving the catalytic activity for oxidation of CO (dos Santos Xavier et al., 2015). High Nd content (0.2 – 0.3) promoted sintering and retarded the catalytic activity of Ce-Zr-Nd catalyst for CO oxidation.

Other catalysts

Aromatic organic chemical tetrapyrrole (commonly known as corrole) combined with transition metals (corX; X standing for the transition metal) have also been used for catalytic oxidation of CO.

 doi:10.20944/preprints202310.0528.v1



In one study, the metals Al, Ga, Si, Ge and As were tested (Mohajeri and Hassani, 2018). The best results were obtained from the CorAl and CorGa while CorSi and CorGe formed very stable carbon-like intermediates that hindered CO oxidation. Other researchers have used $Li_5FeO_4$ and $LiFeO_2$ (Lara-García et al., 2017), V/graphene (Tang et al., 2018), Cr/graphene (Dai et al., 2018), and $ZrO_2$/MgO for oxidation of CO.

The ideal catalyst for CO oxidation should have high selectivity, high activity, thermally stable and long life, all of which come at a high cost. Noble metals are the best choice, but they are very expensive. Research into new materials such as Mn, Fe, Co, Ni, Cu or their combinations has been extensive (Rola Mohammad et al., 2018), however, improving their stability is still a challenge. Even the reaction itself between CO and $O_2$ on catalyst surfaces has had over 20 different proposed mechanisms with the Langumir–Hinshelwood (LH) being the best. Understanding the dynamic reactions at microscopic level on surface and the bulk of the catalyst under heating and cooling is the task at hand for researchers.

### *4.4. CO detection technologies/sensors*

#### 4.4.1. Sensors

The development of CO sensors started in the mid-1900s, but the actual reported sensors became operational in the 1970-1980s (Windischmann and Mark, 1979). The early designs had chemical pads that changed to a brownish or blackish color when exposed to CO. As CO related deaths became rampant, audible alarms became the standard. The alarm response on the CO detector uses a concentration-time function. Lower CO concentrations would not trigger the alarm for a given period, however, higher CO levels would cause the alarm to go off in a few minutes. This concentration-time function mimics the CO assimilation in the body while preventing false alarms due to common sources of CO like cigarette smoke.

#### Colorimetric CO sensors

Several sensors have been designed especially using mono, di, and tri-rhodium complexes. Binuclear rhodium complexes $[Rh_2\{(XC_6H_3)P(XC_6H_4)\}n(OCR)_2]$, when exposed to 100-300 ppm CO would change from purple to red within 20 seconds at room temperature (Pannek et al., 2018). A potassium-palladium complex ($K_2Pd(SO_3)_2$) with a high response at room temperature would have a detection limit of 1 ppm (Lin et al., 2018). Similarly, a Rh complex activated with ethanol and tributyl phosphate would also change from purple to red upon exposure to only 10 ppm CO within 30-60 seconds. Some designs are even more sensitive that they can detect CO levels as low as 5 ppb at room temperature (Toscani et al., 2015).

Ruthenium (II) complexes react extensively with small-donor ligands such as CO. This concept was used to design CO colorimetric probe which expresses both chromo- and fluorogenic response. At low CO levels as 5 ppb, a color response could be observed by the naked eye with clear changes from orange to yellow seen at 100 ppm of CO in air. When the turn-on emission fluorescence was increased, substantial sensitivity to 1 ppb of CO could be achieved in air and in solution. The system is insensitive to moisture and other gases (Moragues et al., 2014).

Preprints (www.preprints.org) | NOT PEER-REVIEWED | Posted: 10 October 2023 doi:10.20944/preprints202310.0528.v1



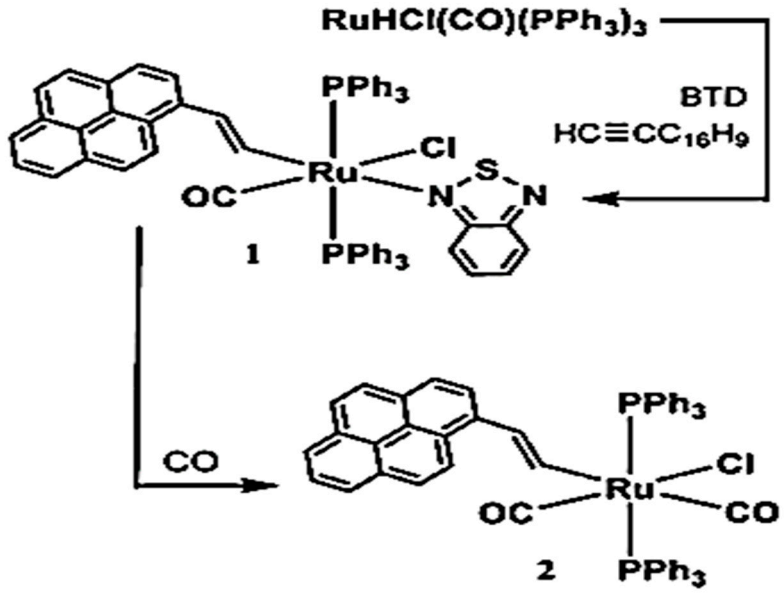


**Figure 12.** Formation of the Complexes [Ru(CH=CHPyr1)Cl(CO)(BTD) $(PPh_3)_2$] (1) and [Ru(CH=CHPyr1)$Cl(CO)_2(PPh_3)_2$] (2)*(Moragues et al., 2014)*.

Electrochemical

These fuel cells produce a signal current that is proportional to the concentration of the target gas (i.e. CO). The electrochemical cell has a container, the working and counter electrodes, connection wires and an electrolyte – usually an acid. The oxygen available at one electrode is used to oxidise CO at the other electrode to carbon dioxide which is detected. Electrochemical cells have high accuracy and linear output to CO concentration, require minimal power, are operated at room temperature, and have a long lifetime (i.e. ≥5 years).

At the onset of the 1980's, (Okamoto et al., 1980) developed an electrochemical sensor based on Yttria-stabilized zirconia as the electrolyte and Pt electrodes. For 160 ppm of CO, it took 300 seconds for the sensor emf to reach 90% of its saturation at 300 °C. Ten years later, (Otagawa et al., 1990) used a Nafion® membrane as an electrolyte with Pt electrodes to design a CO sensor that could detect 500 ppm of CO within 100 seconds at 20-22 °C. Towards the end of the 20th century, (Tess and Cox, 1998) developed a silica electrolyte based sensor with Pt electrodes that could detect 67 ppm of CO within 2-50 seconds at 20-22 °C.

In 2007, (Santhosh et al., 2007) showed that a multiwall carbon nanotubes and poly-diphenylamine on a glassy carbon working electrode and Pt counter electrode would work with $HClO_4$, $H_2SO_4$, HCl and $H_3PO_4$ electrolyte to detect 100 ppm of CO within 2 seconds at room temperature. Two years later, (Paul et al., 2009), used a polypyrrole/Au/standard calomel working electrode and Pt counter electrode to design CO electrochemical cell with pyrrole monomer dissolved in acetonitrile and tetrabutylammonium perchlorate as an electrolyte. The sensor could detect 300 ppm of CO at room temperature within <1 second. (Zhi et al., 2012) observed that a cell constructed from $La(CH_3COO)_3{\cdot}1.5H_2O$, $Sr(CH_3COO)_2{\cdot}0.5H_2O$ and $Mn(CH_3COO)_2{\cdot}4H_2O$ (Pt) as working electrode and Yttria-stabilized zirconia as electrolyte could detect 200-500 ppm CO at 550 °C within 65-80 seconds (*Figure 13*). In the same year, (Phawachalotorn et al., 2012) observed that a $RuO_2$ (Pt) working electrode cell with Au (Pt) as counter electrode and $La_{0.8}Sr_{0.2}Ga_{0.8}Mg_{0.2-x}Fe_xO_3$ and $La_{0.8}Sr_{0.2}Ga_{1-x}Fe_xO_3$ as electrolyte could be used to detect 1000 ppm of CO at 400 °C within just 120 – 180 seconds.

Preprints (www.preprints.org) | NOT PEER-REVIEWED | Posted: 10 October 2023 doi:10.20944/preprints202310.0528.v1



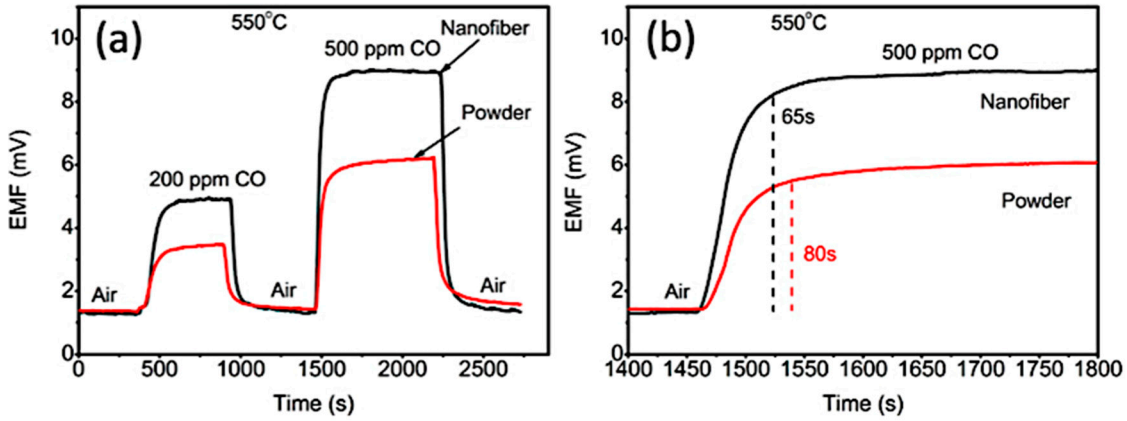


**Figure 13.** Response to change in CO concentration at 550 °C for the nanofiber sensor and the powder sensor (a) and response time (b) (Zhi et al., 2012).

Using pure single-walled carbon nanotube (SWCNT), CuCl-doped SWCNT, and pure CuCl (Zhang et al., 2013) as working electrodes and Au as a counter electrode with $SiO_2$/Si as the electrolyte, a CO electrochemical sensor was constructed. They observed that 20-100 ppm CO could easily be detected at room temperature. (Zhu et al., 2015) realized that PdO powder & $\alpha$-terpineol as working electrode and Pt as a counter electrode with yttria-stabilized zirconia could be a good combination for detection of CO. They observed that 20-200 ppm of CO could be detected in 118 seconds at 450 °C. In 2016, (Izu et al., 2016) used Pt for both working and counter electrodes with zirconia-doped ceria ($Ce_{0.9}Zr_{0.1}O_2$) as the electrolyte and observed that 1000-5000 ppm of CO could be detected in 2-4 seconds at 400-500 °C. In the same year, (Shimizu et al., 2016) used Au/$SnO_2$ as working electrode and Au as a counter electrode with anion-conducting polymer as the electrolyte for a CO sensor. They observed that 10-3000 ppm of CO could be detected in14-300 seconds at 30 °C. All these developments show a remarkable stride in improving the detection of CO with electrochemical sensors.

Semiconductor

The circuit system of semiconductor sensors consists of thin wires of the semiconductor material on an insulating ceramic base. This sensing element is heated to an appropriate temperature for proper operation. Exposure to CO would reduce the resistance while oxygen would increase it. The integrated circuit works by monitoring the resistance of the sensing element (Bornand, 1983). Semiconductor sensors have a longer shelf life (i.e. >10 years), however, they require higher power compared to electrochemical sensors.

In 1983, (Bornand, 1983) developed a tin oxide sensor with Ag & Au electrodes to detect 1750 ppm of CO within 100 seconds at 400-600 °C. Five years later, (Formosa et al., 1988) developed a Pd-gate sensor that could detect 10,000 ppm of CO at <200 °C within 60 seconds. In 1994, (Cantalini et al., 1994) developed an $\alpha$-$Fe_2O_3$ microporous ceramic sensor that was very sensitive to 300 ppm of CO at 300-400 °C. (Davis et al., 1998) investigated the effects of crystallite growth and dopant migration on the CO detection properties of nanocrystalline $SnO_2$ sensor in 1998. They observed that 300 ppm of CO could be detected very fast if the sensor was tuned to 200 – 400 °C temperature.

In 2002, (Sin et al., 2002) also investigated the sensing properties of $SnO_2$-Cu/Pt/$SiO_2$ for 1000 ppm of CO. The developed sensor could detect CO within 5 seconds at 270-320 °C. In 2006, (Wang et al., 2006) used Au/Sn sensors-based gold/tin dioxide, to detect 500 ppm of CO within 30-70 seconds at 81-210 °C. In 2011, (Blondeau-Patissier et al., 2011) investigated the surface acoustic wave devices in combination with Cobalt corroles to detect 4.5 ppm CO at room temperature. The sensor was able to detect the low-level CO within 100 seconds. (Anastasescu et al., 2016), found out that a $SnO_2$–ZnO sensor could detect 50-2000 ppm of CO within 120 seconds at 210 – 300 °C. More recently (P. Kumar et al., 2018) found out that ZnO and Fe-ZnO thin films could detect CO at 100 – 600 °C within 3-5

Preprints (www.preprints.org) | NOT PEER-REVIEWED | Posted: 10 October 2023 doi:10.20944/preprints202310.0528.v1



seconds. This year (2019), (Ortega et al., 2019), observed that europium doped ceria sensors (*Figure 14*) could detect CO at 100 – 400 °C within 56 seconds. More semi-conductor sensors are given in Appendix A - Table 1.

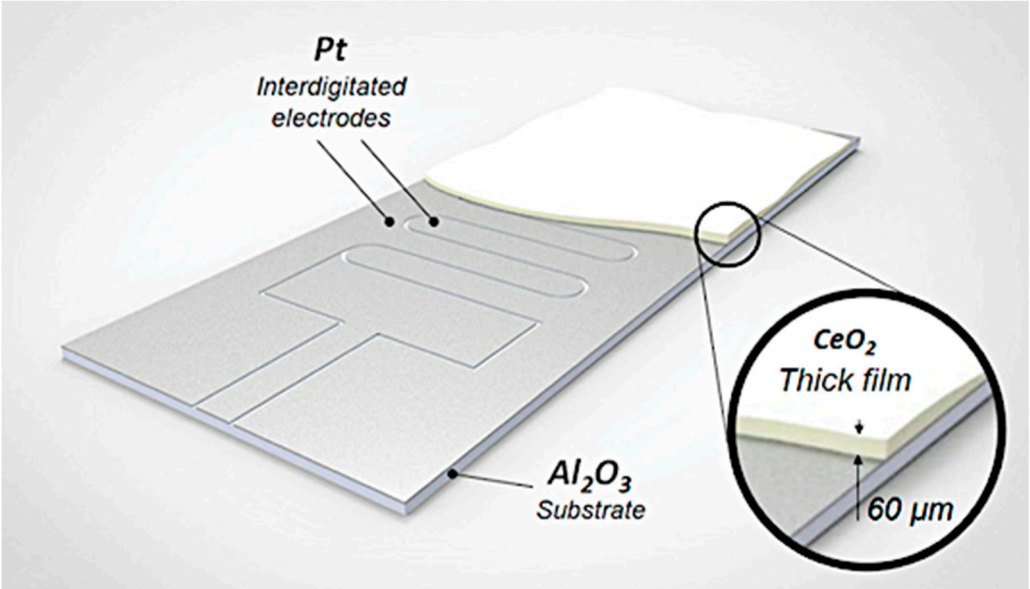


**Figure 14.** Illustration of the deposited ceria film on alumina substrates with interdigitated Pt electrodes (Ortega et al., 2019).

Infrared sensors

These sensors work by analyzing the absorption signature wavelength of the target gaseous sample in the electromagnetic spectrum (Li et al., 2012). Carbon monoxide has strong absorption in the 4.6 mm region. (Dong et al., 2017) observed that using a dual-channel pyroelectric detector with a self-developed digital signal processor-based orthogonal lock-in amplifier, they could detect up to 1000 ppm of CO within only seven seconds. (Qiu et al., 2019) used a similar system but with a 32-bit microcontroller and detected 125 ppm of CO within 110 seconds.

Continuous-wave mode distributed feedback quantum cascade laser with optical length, and self-development electronic modules (Dang et al., 2018), have also been used for detecting low levels of CO at ambient temperature (Vanderover and Oehlschlaeger, 2010) with quick responses of up to 3 seconds. Similar quantum cascade laser utilizing mid-infrared (Mulrooney et al., 2008), (Barron-Jimenez et al., 2006) wavelength modulation spectroscopy absorption sensor (Vanderover et al., 2011) and very low limits of detection as 0.03 ppm have also had very quick responses to CO.

Laser diodes with thermoelectric coolers as radiation source (Shanying et al., 2010), (Thurmond et al., 2016) have detected 50-5000 ppm of CO within 20 seconds. Some of these have slightly high detection limits of up to 50 ppm (Zhu et al., 2010). Others use a tunable diode laser spectroscopy sensor with a vertical-cavity surface-emitting laser (Hangauer et al., 2014).

Photoionization detectors (PIDs) with UV-assisted Cataluminescent (CTL) sensor based on g-$C_3N_4$ (Li et al., 2018) and photons platform using a distributed-feedback laser diode operating at room temperature (Thomazy et al., 2010) have been of much success with low detection limits 0.08-3 ppm and response times as a second to as high as 140 seconds.

4.4.2. Wireless systems

Recently, remote warning handsets or strobes, and vibrating pillow pads have been introduced as linkages to wireless safety solutions in homes. These provide warning signals to those with impediments like the deaf, blind and deep sleepers to get up quickly and escape a suspected CO incident in any facility. Metal-oxides like tin oxide ($SnO_2$) semiconductor sensor, a data acquisition system, and a communication system from remote terminal unit to a web server have been used for

 doi:10.20944/preprints202310.0528.v1



CO detection with an average error of 7.73 ppm, and a mean absolute percentage error of only 2.81% (Suryono et al., 2017). With a three-lead electrochemical CO sensor without battery (2.5 W), and the power consumption of only ~13 mW, a wireless system was set up and used with a Nordic Bluetooth dongle low power protocol to send a trigger to activate Wi-Fi alarms and notifications to the mobile device through the Internet (Chen et al., 2016).

Using sensor nodes consisting of an LM35DZ temperature sensor, a humidity sensor HSM 20-G and a CO sensor TGS 2600, can be used to achieve an average error of 4.414% when compared to the dataset and 2.12% (if the data outliers are eliminated) (Firdaus et al., 2016). Chen, Shi, and Guo used Wireless Sensor Network node, low-power microprocessor C8051F930, with CO metal oxide semiconductor sensor to detect CO in the range of 30 to 1000 ppm with a data transmitting distance of 200 m (Chen et al., 2013). (Bicelli et al., 2009) used a similar system but with TGS2442 (Figaro, Inc.) metal-oxide CO sensors to detect CO in the range of 30 to 300 ppm. The sensitivity obtained was <1s, at room temperature.

The challenge with CO sensor systems are mainly false detection due to age, malfunctions or chemical substance with a similar signature as CO (Ryan and Arnold, 2011). Fitting new sensors, and continuous research and development is the only way to solve this challenge.

## 5. Catalyst impregnation on to solid fuels

### *5.1. Enhancing pyrolysis and char gasification*

When secondary reactions are triggered during biomass pyrolysis by either alkali or alkali earth metals (Anca-Couce et al., 2017), the resulting char has varying reactivity. This could be due to blocking or deactivation of active sites for oxygen attack. (Kirtania et al., 2017) observed that impregnation of sawdust with $K_2CO_3$, $Na_2CO_3$, NaOH and NaCl, followed by devolatilising, and pyrolysing the resulting char at different temperatures (750–900 °C) under $CO_2$, three classes of chars were produced. Those chars that were highly influenced by catalysts were swollen and had molten surfaces. The moderately influenced chars were wood-like while the least affected had salt deposits. Potassium carbonate ($K_2CO_3$) gave the best catalytic activity for gasification. When iron or nickel were impregnated on cellulose, the yield and composition of fast pyrolysis products were different compared to un-catalysed cellulose (Collard et al., 2015). With only1.5wt% Fe or 1.7wt% Ni catalyst loading, cellulose depolymerization was inhibited; char, moisture, and $CO_2$ yields were increased while tar and CO yields were reduced.

(Yu et al., 2017), observed that bread waste could be turned into hydroxymethylfurfural (HMF) by impregnation of $SnCl_4$, $AlCl_3$, and $FeCl_3$ followed by pyrolysis. The highest HMF yield (30 mol%) was achieved using $SnCl_4$ as the catalyst (*Figure 15*). The polymerization-induced metal-impregnated high-porosity carbon was a possible precursor of the biochar-based catalyst.

Preprints (www.preprints.org) | NOT PEER-REVIEWED | Posted: 10 October 2023 doi:10.20944/preprints202310.0528.v1



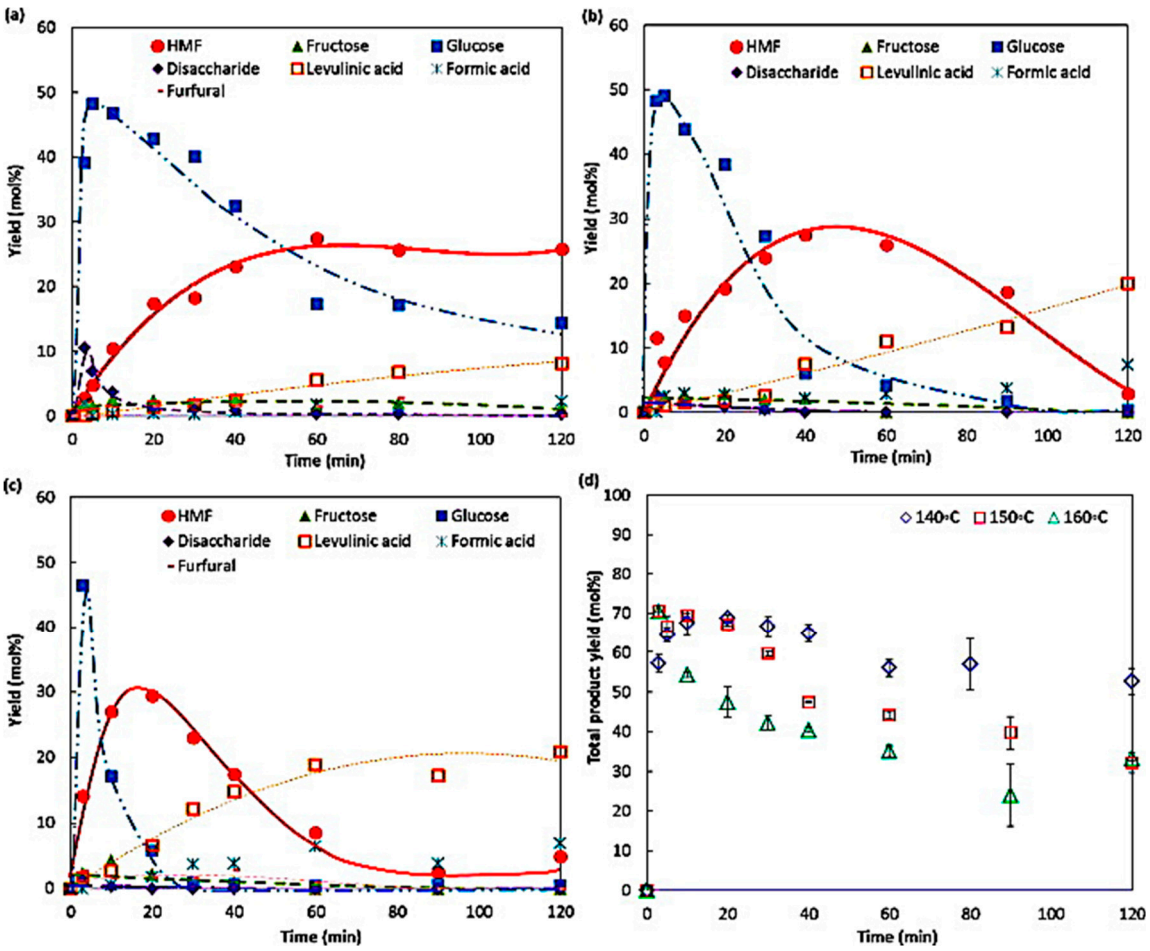


**Figure 15.** Product yields during the $SnCl_4$-mediated conversion of bread waste under heating at (a) 140 °C, (b) 150 °C, and (c) 160 °C; and (d) total product yield at the three temperatures (conditions: 5 wt/v% substrate and 55.5 mM metal chloride in Dimethyl sulfoxide/water (1:1v/v); yield = $product_{Cmol}/substrate_{Cmol}$ x100%) (Yu et al., 2017).

Copper and lead impregnated on biomass had little effect on kinetic parameters that describe the pyrolysis process (Martín-Lara et al., 2016), (Martín-Lara et al., 2018). However, silicon compounds resulted in glassy shelled char (Trubetskaya et al., 2016) when impregnated on rice husk biomass. The particle size and shape of the resulting chars were preserved. However, the reactivity of the char is more influenced by alkali content than the silicon oxides. The presence of K, in the raw biomass increases the reactivity and favoured the heat produced during low-temperature oxidation of the chars. This implies that the self-heating tendency of the char could be reduced by removal of inorganic matter through leaching of the biomass (Fan and Sheng, 2016).

### *5.2. Other applications of catalyst impregnated solid fuels*

#### 5.2.1. Improving char properties and removal of pollutants

Charcoal has been used as a support in several studies and has worked excellently. The addition of Co, Ni, and Fe to charcoal followed pyrolysis under helium enhanced the thermal stability of charcoal for catalytic combustion of volatile organic compounds (Liao et al., 2016). Cobalt gave the best results transforming the amorphous carbon into a graphite-like structure and also served as an active phase in the toluene and ethyl acetate oxidation reaction. Copper impregnated on activated carbon produced from oxytetracycline bacterial residue (Zhou et al., 2015) gave excellent activity for adsorption and oxidation of sulphur dioxide than the activated carbon alone. Similarly, hydrated manganese oxide supported by biochar effectively sequestrate Pb(II) and Cd(II) than biochar alone

Preprints (www.preprints.org) | NOT PEER-REVIEWED | Posted: 10 October 2023 doi:10.20944/preprints202310.0528.v1



(Wan et al., 2018). Interestingly, the catalyst system could be regenerated and re-used several times. The catalyst activity was attributed to specific inner-sphere complexation of the manganese oxide and pre-enrichment and permeation of Pb(II) and Cd(II) cations into the pore channels of biochar enhanced by the oxygen-containing groups.

Coloured pigments are easily removed when char is impregnated with some metal catalysts. (Park et al., 2018) observed that Fe-impregnated sugarcane biochar could achieve a 99.7% azo dye Orange G (OG) efficiency from solution within 2 hours. The Fe- sugarcane-biochar is more economical, efficient, and recyclable. In similar studies, 96% MB dye removal efficiency was achieved using Ni-impregnated powder activated carbon (Alayan et al., 2018) while RB5 azo dye was completely degraded using grape marc activated carbon/$TiO_2$ hybrid (Bourahla et al., 2018) catalyst. The degradation species including carboxylic and sulfate groups were observed on the surfaces of the hybrid catalyst using FT-IR and UV-visible analysis.

(Poggi and Singh, 2016) observed that impregnation of Fluid Cracking Catalyst (FCC) on modified biochar achieved a higher thermal degradation capability of acetic acid than FCC alone. With no catalyst, only 5.55% conversion was achieved. With biochar-Ni, a15.21% conversion was achieved while FCC achieved a 12.41% conversion. The modified bio-char (Biochar-Fe) showed the highest conversion of 40.66%.

5.2.2. Fuel cell performance enhancement

The use of coal char impregnated with iron oxide or calcium oxide for the anode and Y/Zr with $La_{0.8}Sr_{0.2}MnO_3$ as cathode enhanced the performance of the fuel cell even without a catalyst (Jiao et al., 2015). There was a two-fold increase in peak power density with $Fe_mO_n$-alkaline metal supported coal char compared to a cell fuelled with pure coal char alone.

## 6. Conclusions and ideas for future work

This work has discussed solid fuel processing, kinetics and the major advances for minimizing human to exposure to carbon monoxide from solid fuel combustion. In summary;

- Solid fuel processing may be achieved by combustion (smoldering or flaming), thermochemical (torrefaction, flash carbonization, pyrolysis, gasification, hydrothermal or liquefaction), and biochemical (anaerobic digestion, fermentation and photobiological processing),
- The general emission products from combustion of solid fuels may be organic and could include more than 15 inorganic elements. Carbon monoxide is released from oxygenated surface functional groups followed by free edge and zig-zag site reactions on PAHs molecules reacting with oxygen until the entire structure is oxidized.
- The methods used to determine kinetic parameters include among others, Friedman, Gupita, KAS, FWO, Starink, Boswel, Coats and Redfern, ASTM methods, Karaosmanoglu and Cif, isothermal methods, iterative methods and Kissinger. There are also methods for determining entropy ($\Delta S$), pre-exponential factor (A), Gibbs free energy ($\Delta G$), and enthalpy change ($\Delta H$).
- Carbon monoxide has been a silent killer since the paleolithic era and has continued to threaten human lives until today.
- Improved cook-stoves offer high heat conservation with less or no smoke at all. They are highly efficient with natural and forced draft air systems and some employ catalyst layers hence ensuring the safety of users from toxic combustion emissions
- Heating systems with two-stage combustion and improved biomass boilers with/without catalysts have also been very crucial in reducing CO exposure. They achieve up to 80% CO conversion and offer multi-solid-fuel usage designs. They have low energy requirements and could be operated as domestic or for district heating systems

 doi:10.20944/preprints202310.0528.v1



- Direct catalytic oxidation of post-combustion pollutants are highly efficient and can achieve 100% CO conversion at very low catalyst loading and ambient temperature. They can be used in conjunction with other systems like cooking and heating. There are various combinations of catalysts available commercially and many more to be designed in the future. Their success is attributed to their high affinity for oxygen and toxic pollutants onto their surfaces.
- The CO sensor systems are various and offer the portability advantage. They have very low detection limits and quick response times. They operate at ambient temperatures enabling usage in various environments. Lately, they can be incorporated with wireless systems allowing CO detection remotely.

Although substantial safety from CO has been provided by the minimization systems described above, there are still several CO related deaths recorded worldwide. All the systems used to minimize CO exposure apply the solid fuel in their original form and during combustion, such solid fuels continue to release CO depending on the prevailing conditions without being impeded. Should there be any malfunction, leakage or pathway for CO, such systems would still expose the user to toxic amounts that may be lethal or cause lifelong injuries.

Altering the composition of the solid fuels by impregnation of chemical catalysts has been used to trigger desired reactions and achieve target products. Using such an approach on solid fuels used for cooking and heating systems would ensure that the solid fuel release minimal amounts of CO. Hence, the amounts of CO released would be rendered none lethal acutely. This coupled with other technologies like sensors/detectors would ensure a safer environment for solid fuel users.

The challenges envisaged would be the costs added to the solid fuel by impregnation of catalysts. Such products if not well marketed may not compete favorably with non-catalyst impregnated products. Furthermore, there are many other considerations from the health and manufacturing perspectives that would also dictate the final pricing. From a health perspective: how much of the catalyst would end up on the food during cooking from the briquette dust, material transfer via contact, and sparks?; would such amounts be within the recommended daily intake as per local and international health standards?; how about the management of ash from the briquettes after cooking – would this ash be environmentally friendly if discharged without caution?. From the manufacturing perspective: making such solid fuels would involve more than just the addition of the catalysts - it may involve accelerants for quick start-up, white ash to show that the briquettes are hot enough and ready to cook food, binders for holding together all the briquette ingredients, press release for easy removal of briquettes from the mould during production, and fillers that add mass to the briquettes.

All the above parameters would add costs to the final product, but the biggest question is how much does someone's life cost? Ultimately, a safe solid fuel is always less expensive than a life. National governments can also assist such projects by waiving off certain taxes on the raw materials used during manufacturing.

**Acknowledgments:** The authors thank the Gas Safety Trust of the United Kingdom, the Boat Safety Scheme of the United Kingdom and the Katie Haines Memorial Trust for sponsoring this work. Gratitude to Dr. Nathalie Mai for the assistance during the processing of this work.

**Declaration of interest**: None.

Preprints (www.preprints.org) | NOT PEER-REVIEWED | Posted: 10 October 2023 doi:10.20944/preprints202310.0528.v1



## Appendix A

*Appendix A - Table 1: Semi-conductor sensors*

| Working/sensing material | CO conc. (ppm) | Response time (s) | Operating temp (°C) | Ref. |
|---|---|---|---|---|
| Ag-$Co_3O_4$ | 5–1500 | 10-30 | 50–200 | (Molavi and Sheikhi, 2018) |
| Cobalt oxide nanosheet and carbon nanotube film | 200 | 23 | Room temp. | (Dai et al., 2010) |
| Au-doped CoOOH | 1000 | 40 | 60 – 110 | (Zhuiykov, 2008) |
| Cobalt oxide (CoOOH) | 1000 | 60 | 80 | (Wu et al., 2006) |
| Ni and Zn doped $SnO_2$ | 500 | 5-7 | 280 | (Tang et al., 2017) |
| Pd on gallia: tin oxide | 30 | 10 | 300–500 | (Kundu et al., 2018) |
| n-type $Zn_2SnO_4$ | 200 | Quick response | 50 | (Chen et al., 2018) |
| $SnO_2$/CMOS | 200 | Quick response | 375 | (Lackner et al., 2017) |
| Ca-$SnO_2$ | 1 | 10-12 | 350 | (Ghosh et al., 2014) |
| $Pd^{2+}$/$SnO_2$/CNT | 500 | 2 | 100 | (Hu et al., 2014) |
| hydroxypropyl cellulose with Pd/$SnO_2$ | 6-18 | Quick response | 60 | (Kim et al., 2013) |
| V–$SnO_2$ and Au/V–$SnO_2$ | 50-1000 | 5-20 | 125 – 175 | (C. T. Wang et al., 2013) |
| V–$SnO_2$ | 50-500 | 14-19 | 175 | (Wang and Chen, 2010) |
| Si–B–C–N-coated $SnO_2$ | 10 – 120 | 20-60 | 350 – 530 | (Prasad et al., 2010) |
| ultrathin $SnO_2$-films | 300 | 20-30 LOD <5ppm | 250-400 | (Tischner et al., 2008) |
| Pt/SnO,/i- diamond/$p^+$-diamond CAIS (Catalyst/Adsorptive Oxide/lnsulator/Semiconductor)diode | 0.4 – 5.4 torr | 24-28 | 50-500 | (Gurbuz et al., 1998) |
| CaO/$Nb_2O_5$/$SnO_2$ | 30-2800 | Quick response | 100-230 | (Tsai et al., 1995) |
| Si/$SnO_2$, Pd/$SnO_2$, Borosilicate glass/$SnO_2$ | 40-200 | Quick response | 200-400 | (Van Geloven et al., 1991) |
| $SnO_2$ thin film | 1-100 | Quick response | 350 | (Windischmann, 2006) |
| $SnO_2$ /$La_2O_3$, $SnO_2$/$Sb_2O_5$+$La_2O_3$ and $SnO_2$/Pt+Pd | 200 | Quick response | 100-600 | (Malyshev and Pislyakov, 2008) |
| $SnO_2$ thin film | 1000 | 5-20 | 50-250 | (Salehi, 2003) |
| Ti-doped $SnO_2$ | 300 | 18-20 | 150-450 | (Z. Wang et al., 2013) |
| $Co_XO_Y$/$SnO_2$ | 125-2500 | 4.9-40.5 | Room temp. | (Oleksenko et al., 2013) |
| Bismuth ferrite (BiFeO3) | 5-30 | 25 | 270-450 | (Chakraborty and Pal, 2018) |

 doi:10.20944/preprints202310.0528.v1



| | | | | |
|---|---|---|---|---|
| Prism/Au/ZnO | 0.5-100 | Quick response | Room temp. | (Paliwal et al., 2017) |
| $SnO_2$/ZnO | 100-1000 | 120-240 | 470-510 | (Zaikin et al., 2002) |
| pyridyl-functionalized single-walled carbon nanotubes (F-SWCNTs) and iron porphyrin (Fe(tpp)$ClO_4$) | 50-200 | 30-60 | Room temp. | (Savagatrup et al., 2017) |
| ZnO nanoparticles onto 3D graphene Oxide | 1000 | 7 | 200 | (Phuong et al., 2017) |
| $TiO_2$ (Au- $TiO_2$) thin films | 60-125 | 20 | 230-320 | (Joy et al., 2006) |
| TiO2 thin films | 250 | Quick response | 550 | (Dutta et al., 2005) |
| Nb–$TiO_2$ | 1000 | Quick response | 550 – 850 | (Anukunprasert et al., 2005) |
| TiO2, $TiO_2$/$La_2O_3$, $TiO_2$/$La_2O_3$/CuO and $TiO_2$/CuO | 500 | Quick response | 600 | (Savage et al., 2001) |
| ($La_{2-x}$ A'x $Cu_{1-y}$ B'y $O_4$; A' = Sr, Ba, Ce; B' = Zr, x, y = 0–0.2) | 50-600 | Quick response | 300–600 | (Shimizu et al., 2017) |
| (x)$NiFe_2O_4$ (spinel)(1−x) $La_{0.8}Pb_{0.2}Fe_{0.8}Co_{0.2}O_3$ (0≤x≤1) | 10-500 | 60-360 | 125 – 175 | (Maity et al., 2016) |
| $NdFeO_3$ | 0-50,000 | Responsive | Room temp. | (Ho et al., 2011) |
| $LaCoO_3$–$In_2O_3$, $LaCoO_3$–$Bi_2O_3$ and $LaCoO_3$–PdO | 10-40 | ~ 60-360 | 200-300 | (Salker et al., 2005) |
| Pt/$La_{9.0}Si_{5.8}Mn_{0.2}O_{27-\delta}$ | 500 | 10-20 | 30-160 | (Hosoya et al., 2016) |
| LaCoO3 | 500 | 181 | 100 - 550 | (Ding et al., 2015) |
| $La_{0.87}Co_{1.13}O_3$-loaded $Ce_{0.67}Zr_{0.18}Sn_{0.15}O_{2.0}$ | 500 | 20-40 | 130 | (Hosoya et al., 2015) |
| Pt/$Ce_4La_6O_{17}$ | 1-80 | 0.5-1 | 80-180 | (Yang et al., 2019) |
| Pd/$SiO_2$/Si | 10,000 | 10-60 | 150 | (Jelley and Maclay, 1987) |
| $MoO_3$, $MoO_3$/$ZrO_2$ and $MoO_3$/Pd | 0-5000 | 180-1020 | 350-500 | (Azad, 2006) |
| $BaSnO_3$ | 0-50,000 | <120 | 550 – 950 | (Lampe et al., 1995) |
| $LuFe_2O_4$ | 20-30 | 10-60 | 300-600 | (Ghosh et al., 2016) |
| $MgSb_2O_6$ | 0-500 | Quick response | 23-300 | (Guillén-Bonilla et al., 2016) |
| $TiO_2$/Cu under UV illumination | 100 | 1.5-32 | 120-290 | (Nikfarjam and Salehifar, 2015) |
| Cu doped cryptomelane octahedral molecular sieves (Cu-OMS-2) | 10-8000 | 55 | Room temp | (R. Kumar et al., 2018) |
| Au, Pd, and Pt on CoO and $Co_3O_4$ | Up to 10000 | <300 | 50-250 | (Nagai et al., 2013) |
| Nano-$SnO_2$ powder | 5-100 | 8 | 200-500 | (Chen et al., 2012) |
| Pt/$SnO_2$ | 600 | Quick response | 25–350 | (Kocemba and Rynkowski, 2011) |

| | | | | |
|---|---|---|---|---|
| Pt/$SiO_2$SiC transistor sensor | 0-1250 | Quick response | 100-400 | (Becker et al., 2011) |
| Co-Ce oxide | 3vol% | 72 | 90-125 | (Xu et al., 2008) |
| Ag-doped $SnO_2$ | 100-500 | 10-17 | 200 | (Petruk and Kravets, 2007) |

## References


A. Nyombi, M. Williams, R.W., 2019. Reactivity and Free Radical Chemistry of Lilac (Syringa) Charcoal. Energy & Fuels 33, 1227–1235. doi:10.1021/acs.energyfuels.8b03665

Adrian, B., 2011. Coal fire emissions curb children's growth. Environ. Health Perspect. 119, A245. doi:10.1002/cssc.201000448.4.

Ahmad, M.S., Mehmood, M.A., Ye, G., Al-Ayed, O.S., Ibrahim, M., Rashid, U., Luo, H., Qadir, G., Nehdi, I.A., 2017. Thermogravimetric analyses revealed the bioenergy potential of Eulaliopsis binata. Therm. Anal. Calorim. 130, 1237–1247. doi:10.1007/s10973-017-6398-x

Ahmad, W., Noor, T., Zeeshan, M., 2017. Effect of synthesis route on catalytic properties and performance of Co3O4/TiO2 for carbon monoxide and hydrocarbon oxidation under real engine operating conditions. Catal. Commun. doi:10.1016/j.catcom.2016.10.012

Akhtar, A., Krepl, V., Ivanova, T., 2018. A Combined Overview of Combustion, Pyrolysis, and Gasification of Biomass. Energy & Fuels 32, 7294−7318. doi:10.1021/acs.energyfuels.8b01678

Alayan, H.M., Alsaadi, M.A., Das, R., Abo-Hamad, A., Ibrahim, R.K., AlOmar, M.K., Hashim, M.A., 2018. The formation of hybrid carbon nanomaterial by chemical vapor deposition: An efficient adsorbent for enhanced removal of methylene blue from aqueous solution. doi:10.2166/wst.2018.057

Anastasescu, M., Stan, I., Moldovan, C., Gartner, M., Mihaiu, S., Chesler, P., Muscalu, G., Vladut, C., Calderon Moreno, J.M., Hornoiu, C., Firtat, B., Brasoveanu, C., 2016. Nanostructured SnO2–ZnO composite gas sensors for selective detection of carbon monoxide. Beilstein J. Nanotechnol. 7, 2045–2056. doi:10.3762/bjnano.7.195

Anca-Couce, A., Dieguez-Alonso, A., Zobel, N., Berger, A., Kienzl, N., Behrendt, F., 2017. Influence of Heterogeneous Secondary Reactions during Slow Pyrolysis on Char Oxidation Reactivity of Woody Biomass. Energy and Fuels 31, 2335-2344. doi:10.1021/acs.energyfuels.6b02350

Anderson, G.Q.A., Fergusson, M.J., 2006. Energy from biomass in the UK : sources , processes and biodiversity implications, in: Lbis. pp. 180–183. doi:10.1111/j.1474-919X.2006.00535.x

Anukunprasert, T., Saiwan, C., Traversa, E., 2005. The development of gas sensor for carbon monoxide monitoring using nanostructure of Nb-TiO2. Sci. Technol. Adv. Mater. 6, 359–363. doi:10.1016/j.stam.2005.02.020

Azad, A.M., 2006. Behavior of a New ZrO2-MoO3 Sensor for Carbon Monoxide Detection. J. Electrochem. Soc. 139, 2913. doi:10.1149/1.2069006

Bai, X., Chai, S., Liu, C., Ma, K., Cheng, Q., Tian, Y., Ding, T., Jiang, Z., Zhang, J., Zheng, L., Li, X., 2017. Insight into Copper Oxide-Tin Oxide Catalysts for the Catalytic Oxidation of Carbon Monoxide: Identification of Active Copper Species and a Reaction Mechanism. ChemCatChem. doi:10.1002/cctc.201700460

Bailis, R., Ezzati, M., Kammen, D.M., 2003. Greenhouse gas implications of household energy technology in Kenya. Environ. Sci. Technol. 37, 2051-2059. doi:10.1021/es026058q

Barron-Jimenez, R., Caton, J.A., Anderson, T.N., Lucht, R.P., Walther, T., Roy, S., Brown, M.S., Gord, J.R., 2006. Application of a difference-frequency-mixing based diode-laser sensor for carbon monoxide detection in the 4.4-4.8 μm spectral region. Appl. Phys. B Lasers Opt. 85, 185–197. doi:10.1007/s00340-006-2281-3

Becker, E., Andersson, M., Eriksson, M., Spetz, A.L., Skoglundh, M., 2011. Study of the sensing mechanism towards carbon monoxide of platinum-based field effect sensors. IEEE Sens. J. 11, 1527–1534. doi:10.1109/JSEN.2010.2099652

Bicelli, S., Depari, A., Faglia, G., Flammini, A., Fort, A., Mugnaini, M., Ponzoni, A., Vignoli, V., Rocchi, S., 2009. Model and experimental characterization of the dynamic behavior of low-power carbon monoxide MOX sensors operated with pulsed temperature profiles, in: IEEE Transactions on Instrumentation and Measurement. IEEE, pp. 1324–1332. doi:10.1109/TIM.2009.2012940

Biemelt, T., Wegner, K., Teichert, J., Lohe, M.R., Martin, J., Grothe, J., Kaskel, S., 2016. Hopcalite nanoparticle catalysts with high water vapour stability for catalytic oxidation of carbon monoxide. doi:10.1016/j.apcatb.2015.11.008

Bignal, K.L., Langridge, S., Zhou, J.L., 2008. Release of polycyclic aromatic hydrocarbons, carbon monoxide and particulate matter from biomass combustion in a wood-fired boiler under varying boiler conditions. Atmos. Environ. 42, 8863–8871. doi:10.1016/j.atmosenv.2008.09.013

Blaine, R.L., Kissinger, H.E., 2012. Homer Kissinger and the Kissinger equation. Thermochim. Acta 540, 1–6. doi:http://dx.doi.org/10.1016/j.tca.2012.04.008

Blondeau-Patissier, V., Vanotti, M., Rabus, D., Ballandras, S., Chkounda, M., Barbe, J.M., Ballandras, S., Rauch, J.Y., 2011. Development of accurate system of gas detection based on love wave sensors functionalized with cobalt corroles applied to the detection of carbon monoxide. Proc. IEEE Sensors 1078–1081. doi:10.1109/ICSENS.2011.6127330

Bornand, E., 1983. Influence of the annealing temperature of non-doped sintered tin dioxide sensors on their sensitivity and response time to carbon monoxide. Sensors and Actuators 4, 613–620. doi:https://doi.org/10.1016/0250-6874(83)85075-6

Borrego, A.G., Garavaglia, L., Kalkreuth, W.D., 2009. Characteristics of high heating rate biomass chars prepared under N2 and CO2 atmospheres. Int. J. Coal Geol. 77, 409-415. doi:10.1016/j.coal.2008.06.004

Borsos, E., Makra, L., Beczib, R., Vitanyi, B., Szentpeteri, M., 2003. Anthropogenic Air pollution in ancient times. Acta Climatol. Chorol. 36–37, 5–15.

Boswell, P.G., 1980. On the calculation of activation energies using a modified Kissinger method. J. Therm. Anal. 18, 353–358. doi:10.1007/BF02055820

Bourahla, S., Harrats, C., Belayachi, H., Nemchi, F., Belhakem, M., 2018. Grape marc activated carbon/TiO2 hybrid degradation of RB5 azo dye: FT-IR and UV-visible analysis. doi:10.5004/dwt.2018.21905

Brennan, L., Owende, P., 2010. Biofuels from microalgae — A review of technologies for production, processing, and extractions of biofuels and co-products. Renew. Sustain. Energy Rev. 14, 557–577. doi:10.1016/j.rser.2009.10.009

Byul, S., Kyu, K., Choi, S., Hee, H., Han, L.G., 2018. Analysis of Emission Characteristics and Emission Factors of Carbon Monoxide and Nitrogen Oxide Emitted from Wood Pellet Combustion in Industrial Wood Pellet Boilers Supplied According to the Subsidy Program of Korea Forest Service. J. Korean Wood Sci. Technol. 46, 597–609. doi:https://doi.org/10.5658/WOOD.2018.46.5.597

Calvo, A.I., Martins, V., Nunes, T., Duarte, M., Hillamo, R., Teinilä, K., Pont, V., Castro, A., Fraile, R., Tarelho, L., Alves, C., 2015. Residential wood combustion in two domestic devices: Relationship of different parameters throughout the combustion cycle. Atmos. Environ. 116, 72–82. doi:10.1016/j.atmosenv.2015.06.012

Cantalini, C., Faccio, M., Ferri, G., Pelino, M., 1994. The influence of water vapour on carbon monoxide sensitivity of $\alpha$-Fe2O3 microporous ceramic sensors. Sensors Actuators B. Chem. 19, 437–442. doi:10.1016/0925-4005(93)01032-Y

Cao, J.-L., Li, G.-J., Wang, Y., Sun, G., Wang, X.-D., Hari, B., Zhang, Z.-Y., 2014. Mesoporous Co-Fe-O nanocatalysts: Preparation, characterization and catalytic carbon monoxide oxidation. doi:10.1016/j.jece.2014.01.020

Caposciutti, G., Antonelli, M., 2018. Experimental investigation on air displacement and air excess effect on CO, CO2 and NOx emissions of a small size fixed bed biomass boiler. Renew. Energy 116, 795–804. doi:10.1016/j.renene.2017.10.001

Capros, P., Paroussos, L., Fragkos, P., Tsani, S., Boitier, B., Wagner, F., Busch, S., Resch, G., Blesl, M., Bollen, J., 2014. European decarbonisation pathways under alternative technological and policy choices : A multi-model analysis. Energy Strateg. Rev. 2, 231–245. doi:10.1016/j.esr.2013.12.007

Carltonbird, M., Eaimsumang, S., Pongstabodee, S., Boonyuen, S., Smith, S.M., Luengnaruemitchai, A., 2018. Effect of the exposed ceria morphology on the catalytic activity of gold/ceria catalysts for the preferential oxidation of carbon monoxide. Chem. Eng. J. doi:10.1016/j.cej.2018.03.111

Carroll, J.P., Finnan, J.M., Biedermann, F., Brunner, T., Obernberger, I., 2015. Air staging to reduce emissions from energy crop combustion in small scale applications. Fuel 155, 37–43. doi:10.1016/j.fuel.2015.04.008

Chakraborty, S., Pal, M., 2018. Highly efficient novel carbon monoxide gas sensor based on bismuth ferrite nanoparticles for environmental monitoring. New J. Chem. 42, 7188–7196. doi:10.1039/c8nj01237g

Char, C., Graphite, N., 2017. Experimental Model Development of Oxygen-Enriched Combustion Kinetics on Porous Coal Char and Non-Porous Graphite. doi:10.3390/en10091436

Chen, C.C., Sung, G.N., Chen, W.C., Kuo, C.T., Chue, J.J., Wu, C.M., Huang, C.M., 2016. A wireless and batteryless intelligent carbon monoxide sensor. Sensors (Switzerland) 16, 1–11. doi:10.3390/s16101568

Chen, D., Zheng, Z., Fu, K., Zeng, Z., Wang, J., Lu, M., 2015. Torrefaction of biomass stalk and its effect on the yield and quality of pyrolysis products. Fuel 159, 27–32. doi:10.1016/j.fuel.2015.06.078

Chen, W., Zhou, Q., Wan, F., Gao, T., 2012. Gas Sensing Properties and Mechanism of Nano-SnO2-Based Sensor for Hydrogen and Carbon Monoxide. J. Nanomater. 2012, 1–9. doi:10.1155/2012/612420

Chen, Y.C., Shen, Y.R., Hsiao, C.L., 2018. A carbon monoxide interdigitated-capacitor gas sensor based upon a n-type Zn2SnO4 thin film. J. Mater. Sci. Mater. Electron. 29, 1658–1663. doi:10.1007/s10854-017-8078-9

Chen, Z., Shi, Z., Guo, Q., 2013. Design of wireless sensor network node for carbon monoxide monitoring. Telecommun. Syst. 53, 47–53. doi:10.1007/s11235-013-9675-4

Clark, M.L., Peel, J.L., Burch, J.B., Nelson, T.L., Robinson, M., Conway, S., Bachand, A.M., Reynolds, S.J., Clark, M.L., Peel, J.L., Burch, J.B., Nelson, T.L., Robinson, M.M., Conway, S., Bachand, A.M., Reynolds, S.J., 2009. Impact of improved cookstoves on indoor air pollution and adverse health effects among Honduran women. Int. J. Environ. Heal. Res. 19, 357–368. doi:10.1080/09603120902842705

CO-Gas-Safety, 2015a. Fuel type relating to UK Deaths from unintentional carbon monoxide & appliance type relating to UK Deaths from unintentional carbon monoxide.

CO-Gas-Safety, 2015b. Carbon monoxide - Death and injuries.

Coffey, E.R., Muvandimwe, D., Hagar, Y., Wiedinmyer, C., Kanyomse, E., Piedrahita, R., Dickinson, K.L., Oduro, A., Hannigan, M.P., 2017. New Emission Factors and Efficiencies from in-Field Measurements of Traditional and Improved Cookstoves and Their Potential Implications. Environ. Sci. Technol. 51, 12508-12517. doi:10.1021/acs.est.7b02436

Collard, F.-X., Bensakhria, A., Drobek, M., Volle, G., Blin, J., 2015. Influence of impregnated iron and nickel on the pyrolysis of cellulose. doi:10.1016/j.biombioe.2015.04.032

Combustor, B., 2016. Effect of Air Staging Ratios on the Burning Rate and Emissions in an Underfeed Fixed-Bed. Energies 940, 1–16. doi:10.3390/en9110940

Dai, C.L., Chen, Y.C., Wu, C.C., Kuo, C.F., 2010. Cobalt oxide nanosheet and CNT micro carbon monoxide sensor integrated with readout circuit on chip. Sensors 10, 1753–1764. doi:10.3390/s100301753

Dai, G., Chen, L., Zhao, X., 2018. Catalytic oxidation mechanisms of carbon monoxide over single and double vacancy Cr-embedded graphene. doi:10.1007/s10853-018-2896-x

Dang, J., Yu, H., Zheng, C., Wang, L., Sui, Y., Wang, Y., 2018. Development a low-cost carbon monoxide sensor using homemade CW-DFB QCL and board-level electronics. Opt. Laser Technol. 101, 57–67. doi:10.1016/j.optlastec.2017.10.037

Danvirutai, C., Noisong, P., 2015. Combined facile methods of the DSC and origin lab program to study the dehydration kinetics of KMnPO4.H2O. Therm. Anal. Calorim. 2249–2255. doi:10.1007/s10973-014-4319-9

Davis, S.R., Chadwick, A. V., Wright, J.D., 1998. The effects of crystallite growth and dopant migration on the carbon monoxide sensing characteristics of nanocrystalline tin oxide based sensor materials. J. Mater. Chem. A 8, 2065–2071. doi:10.1088/0022-3735/20/9/311

Ding, J.C., Li, H.Y., Cai, Z.X., Zhang, X.D., Guo, X., 2015. LaCoO3-based sensors with high sensitivity to carbon monoxide. RSC Adv. 5, 65668–65673. doi:10.1039/c5ra10521h

Dong, M., Zheng, C., Miao, S., Song, F., Wang, Y., 2017. A mid-infrared carbon monoxide sensor system using wideband absorption spectroscopy and a single-reflection spherical optical chamber. Infrared Phys. Technol. 85, 450–456. doi:10.1016/j.infrared.2017.08.006

dos Santos Xavier, L.P., Rico-Pérez, V., Hernández-Giménez, A.M., Lozano-Castelló, D., Bueno-López, A., 2015. Simultaneous catalytic oxidation of carbon monoxide, hydrocarbons and soot with Ce-Zr-Nd mixed oxides in simulated diesel exhaust conditions. doi:10.1016/j.apcatb.2014.07.013

Du, P.-P., Hu, X.-C., Wang, X., Ma, C., Du, M., Zeng, J., Jia, C.-J., Huang, Y.-Y., Si, R., 2017. Synthesis and metal-support interaction of subnanometer copper-palladium bimetallic oxide clusters for catalytic oxidation of carbon monoxide. Inorg. Chem. Front. doi:10.1039/c6qi00535g

Dutta, P.K., Frank, M., Hunter, G.W., George, M., 2005. Reactively sputtered titania films as high temperature carbon monoxide sensors. Sensors Actuators, B Chem. 106, 810–815. doi:10.1016/j.snb.2004.09.036

Ezzati, M., Mbinda, B.M.B.M., Kammen, D.M.D.M., 2000. Comparison of emissions and residential exposure from traditional and improved cookstoves in Kenya. Environ. Sci. Technol. 34, 578-583. doi:10.1021/es9905795

Fan, S., Sheng, C., 2016. Impact of Inorganic Matter on the Low-Temperature Oxidation of Cornstalk and Cellulose Chars. Energy and Fuels 30, 1783–1791. doi:10.1021/acs.energyfuels.5b02287

Fedunik-hofman, L., Bayon, A., Hinkley, J., Lipin, W., 2019. Friedman method kinetic analysis of CaO-based sorbent for high-temperature thermochemical energy storage. Chem. Eng. Sci. 200, 236–247. doi:https://doi.org/10.1016/j.ces.2019.02.003

Fernandez, A., Mazza, G., Rodriguez, R., 2017. Thermal decomposition under oxidative atmosphere of lignocellulosic wastes : Different kinetic methods application. J. Environ. Chem. Eng. 6, 404–415. doi:doi.org/10.1016/j.jece.2017.12.013

Firdaus, Ahriman, N., Yulianto, A., Kusriyanto, M., 2016. Wireless sensor network application for carbon monoxide monitoring, in: Proceeding of the 2015 9th International Conference on Telecommunication Systems Services and Applications, TSSA 2015. IEEE, pp. 1–4. doi:10.1109/TSSA.2015.7440434

Formosa, M., Jelley, K.W., Nowroozi-esfahani, S., 1988. The response of MOS sensors with ultrathin palladium gates to carbon monoxide and methane. Sensors and Actuators 14, 331–348. doi:10.1016/0250-6874(88)80023-4

Gas Safety Trust - UK, 2019. Carbon monoxide Gas Safety Statistics on death and Injuries - 2019.

Gas Safety Trust - UK, 2018. Notes relating to the compilation of CO-Gas Safety statistics and graphic representations: Fuel Type relating to UK deaths from unintentional CO poisoning.

Gas Safety Trust - UK, 2017. UK deaths caused by accidental Carbon Monoxide (CO) poisoning. Isle of Wight.

Ghosh, S., Chowdhury, U., Roy, S., Bandyopadhyay, R., 2016. Detection of low ppm carbon monoxide with charge ordered LuFe 2 O 4 gas sensor – A novel sensing mechanism. Ceram. Int. 42, 14944–14948. doi:10.1016/j.ceramint.2016.06.135

Ghosh, S., Narjinary, M., Sen, A., Bandyopadhyay, R., Roy, S., 2014. Fast detection of low concentration carbon monoxide using calcium-loaded tin oxide sensors. Sensors Actuators, B Chem. 203, 490–496. doi:10.1016/j.snb.2014.06.111

Guillén-Bonilla, H., Flores-Martínez, M., Rodríguez-Betancourtt, V.M., Guillen-Bonilla, A., Reyes-Gómez, J., Gildo-Ortiz, L., de la Luz Olvera Amador, M., Santoyo-Salazar, J., 2016. A novel gas sensor based on MgSb2O6 nanorods to indicate variations in carbon monoxide and propane concentrations. Sensors (Switzerland) 16, 1–12. doi:10.3390/s16020177

Gunnell, D., Coope, C., Fearn, V., Wells, C., Chang, S.-S., Hawton, K., Kapur, N., 2015. Suicide by gases in England and Wales 2001-2011: Evidence of the emergence of new methods of suicide. Affect. Disord. 170, 190-195. doi:10.1016/j.jad.2014.08.055

Gupta, A.K., Jena, A.K., Chaturvedi, M.C., 1988. A differential technique for the determination of the activation energy of precipitation reactions from differential scanning calorimetric data. Scr. Metall. 22, 369–371.

Gurbuz, Y., Kang, W.P., Davidson, J.L., Zhou, Q., Kerns, D. V., Henderson, T., 1998. A new high temperature solid-state microelectronic carbon monoxide gas sensor, in: 1998 4th International High Temperature Electronics Conference, HITEC 1998. pp. 230–233. doi:10.1109/HITEC.1998.676793

Hadden, R.M., Rein, G., Belcher, C.M., 2013. Study of the competing chemical reactions in the initiation and spread of smouldering combustion in peat. Proc. Combust. Inst. 34, 2547–2553. doi:10.1016/j.proci.2012.05.060

Hangauer, A., Chen, J., Strzoda, R., Fleischer, M., Amann, M.-C., 2014. Performance of a fire detector based on a compact laser spectroscopic carbon monoxide sensor. Opt. Express 22, 13680. doi:10.1364/oe.22.013680

He, F., Yi, W., Li, Y., Zha, J., Luo, B., 2014. Effects of fuel properties on the natural downward smoldering of piled biomass powder: Experimental investigation. Biomass and Bioenergy 67, 288–296. doi:10.1016/j.biombioe.2014.05.003

Hernik, B., Jagodzi´nska, K., Matuszek, D., 2018. Numerical studies on the influence of air staging on the temperature of flue gas and emission of gases in the combustion chamber of OP 230 boiler. Chem. Process Eng. 39, 59–74. doi:10.24425/119099

Ho, T.G., Ha, T.D., Pham, Q.N., Giang, H.T., Do, T.A.T., Nguyen, N.T., 2011. Nanosized perovskite oxide NdFeO3 as material for a carbon-monoxide catalytic gas sensor. Adv. Nat. Sci. Nanosci. Nanotechnol. 2. doi:10.1088/2043-6262/2/1/015012

Hong, X., Sun, Y., 2016. Effect of Preparation Methods on the Performance of Pt/CeO2 Catalysts for the Catalytic Oxidation of Carbon Monoxide. Catal. Letters. doi:10.1007/s10562-016-1828-0

Hosoya, A., Tamura, S., Imanaka, N., 2016. A Catalytic Combustion-type Carbon Monoxide Gas Sensor Incorporating an Apatite-type Oxide. ISIJ Int. 56, 1634–1637. doi:10.2355/isijinternational.isijint-2016-240

Hosoya, A., Tamura, S., Imanaka, N., 2015. A New Catalytic Combustion-type Carbon Monoxide Gas Sensor Employing Precious Metal-free CO Oxidizing Catalyst. ISIJ Int. 55, 1699–1701. doi:10.2355/isijinternational.isijint-2015-134

Hu, Q., Liu, S., Lian, Y., 2014. Sensors for carbon monoxide based on Pd/SnO2/CNT nanocomposites. Phys. Status Solidi Appl. Mater. Sci. 211, 2729–2734. doi:10.1002/pssa.201431392

Hu, Z.-P., Zhu, Y.-P., Gao, Z.-M., Wang, G., Liu, Y., Liu, X., Yuan, Z.-Y., 2016. CuO catalysts supported on activated red mud for efficient catalytic carbon monoxide oxidation. Chem. Eng. J. doi:10.1016/j.cej.2016.05.008

Izu, N., Matsubara, I., Itoh, T., Shin, W., 2016. Performance of a carbon monoxide sensor based on zirconia-doped ceria. J. Asian Ceram. Soc. 4, 205–208. doi:10.1016/j.jascer.2016.04.001

Jamali, T., Fatmi, Z., Shahid, A., Khoso, A., 2017. Evaluation of short-term health effects among rural women and reduction in household air pollution due to improved cooking stoves : quasi experimental study. Air Qual. Atmos. Heal. 10, 809–819. doi:10.1007/s11869-017-0481-0

Jeguirim, M., Said, R., Trouvé, G., El may, Y., Dorge, S., 2012. Experimental investigation on gaseous emissions from the combustion of date palm residues in laboratory scale furnace. Bioresour. Technol. 131, 94–100. doi:10.1016/j.biortech.2012.12.120

Jelley, K.W., Maclay, G.J., 1987. A Dual-Mechanism Carbon-Monoxide and Hydrogen Sensor Utilising an Ultrathin Layer of Palladium. IEEE Trans. Electron Devices 34, 2086–2097. doi:10.1109/T-ED.1987.23202

Jenkins, B.M., Baxter, L.L., Jr, T.R.M., Miles, T.R., 1998. Combustion properties of biomass. Fuel Process. Technol. 54, 17–46. doi:10.1016/S0378-3820(97)00059-3

Jerez, A., 1983. A modification to the freeman and carroll method for the analysis of the kinetics of non-isothermal processes. J. Therm. Anal. 26, 315–318.

Jetter, J., Zhao, Y., Smith, K.R., Khan, B., Decarlo, P., Hays, M.D.M.D., Yelverton, T., Decarlo, P., Hays, M.D.M.D., 2012. Pollutant emissions and energy efficiency under controlled conditions for household biomass cookstoves and implications for metrics useful in setting international test standards. Environ. Sci. Technol. 46, 10827-10834. doi:10.1021/es301693f

Jiao, Y., Tian, W., Chen, H., Shi, H., Yang, B., Li, C., Shao, Z., Zhu, Z., Li, S.-D., 2015. In situ catalyzed Boudouard reaction of coal char for solid oxide-based carbon fuel cells with improved performance. doi:10.1016/j.apenergy.2014.12.048

Johansson, L.S., Leckner, B., Gustavsson, L., Cooper, D., Tullin, C., Potter, A., 2004. Emission characteristics of modern and old-type residential boilers fired with wood logs and wood pellets. Atmos. Environ. 38, 4183–4195. doi:10.1016/j.atmosenv.2004.04.020

Joseph, F.H., Leo, W.A., 1966. A quick, direct method for the determination of activation energy from thermogravimetric data. Polym. Lett. 4, 323–328. doi:https://doi.org/10.1002/pol.1966.110040504

Joy, T., Wojtek, W., Kourosh, K.-Z., Peter, L., 2006. Carbon monoxide gas sensor based on titanium dioxide nanocrystalline with a langasite substrate. Proc. IEEE Sensors 228–231. doi:10.1109/ICSENS.2007.355763

Juszczak, M., 2014. Concentrations of carbon monoxide and nitrogen oxides from a 25 kw boiler supplied periodically and continuously with wood pellets. Chem. Process Eng. 35, 163–172. doi:10.2478/cpe-2014-0012

Juszczak, M., Cichy, W., Pałaszyńska, K., 2016. Usefulness assessment of automatic air flow control system with oxygen sensor in a 20 kW boiler with periodic wood pellet supply. Drewno 59. doi:10.12841/wood.1644-3985.174.08

Juszczak, M., Lossy, K., 2012. Pollutant emission from a heat station supplied with agriculture biomass and wood pellet mixture. Chem. Process Eng. 33, 231–242. doi:10.2478/v10176-012-0020-3

Khodaei, H., Guzzomi, F., Patiño, D., Rashidian, B., Yeoh, G.H., 2017. Air staging strategies in biomass combustion-gaseous and particulate emission reduction potentials. Fuel Process. Technol. 157, 29–41. doi:10.1016/j.fuproc.2016.11.007

Kim, B., Lu, Y., Hannon, A., Meyyappan, M., Li, J., 2013. Low temperature Pd/SnO2 sensor for carbon monoxide detection. Sensors Actuators, B Chem. 177, 770–775. doi:10.1016/j.snb.2012.11.020

Kirtania, K., Axelsson, J., Matsakas, L., Christakopoulos, P., Umeki, K., Furusjö, E., 2017. Kinetic study of catalytic gasification of wood char impregnated with different alkali salts. doi:10.1016/j.energy.2016.10.134

Kissinger, H.E., 1956. Variation of peak temperature with heating rate in differential thermal analysis. J. Res. Natl. Bur. Stand. (1934). 57, 217. doi:10.6028/jres.057.026

Kocemba, I., Rynkowski, J., 2011. The influence of catalytic activity on the response of Pt/SnO2 gas sensors to carbon monoxide and hydrogen. Sensors Actuators, B Chem. 155, 659–666. doi:10.1016/j.snb.2011.01.026

Koizumi, K., Nobusada, K., Boero, M., 2015. Reaction Pathway and Free Energy Landscape of Catalytic Oxidation of Carbon Monoxide Operated by a Novel Supported Gold-Copper Alloy Cluster. doi:10.1021/acs.jpcc.5b04223

Kucharczyk, B., 2015. Catalytic Oxidation of Carbon Monoxide on Pd-Containing LaMnO3 Perovskites. doi:10.1007/s10562-015-1518-3

Kumar, P., Samiksha, S., Gill, R., 2018. Carbon Monoxide Gas Sensor Based on Fe-ZnO Thin Film. Asian J. Chem. 30, 2737–2742. doi:https://doi.org/10.14233/ajchem.2018.21574

Kumar, R., Mittal, J., Kushwaha, N., Rao, B. V., Pandey, S., Liu, C.P., 2018. Room temperature carbon monoxide gas sensor using Cu doped OMS-2 nanofibers. Sensors Actuators, B Chem. 266, 751–760. doi:10.1016/j.snb.2018.03.182

Kundu, S., Sudharson, R., Narjinary, M., 2018. Pd impregnated gallia: tin oxide nanocomposite—An excellent high temperature carbon monoxide sensor. Sensors Actuators, B Chem. 254, 437–447. doi:10.1016/j.snb.2017.07.094

Lackner, E., Krainer, J., Wimmer-Teubenbacher, R., Sosada, F., Deluca, M., Gspan, C., Rohracher, K., Wachmann, E., Köck, A., 2017. Carbon monoxide detection with CMOS integrated thin film SnO2 gas sensor. Mater. Today Proc. 4, 7128–7131. doi:10.1016/j.matpr.2017.08.007

Lamberg, H., Sippula, O., Tissari, J., Jokiniemi, J., 2011. Effects of Air Staging and Load on Fine-Particle and Gaseous Emissions from a Small-Scale Pellet Boiler. Energy & Fuels 25, 4952–4960. doi:10.1021/ef2010578

Lamberg, H., Sippula, O., Tissari, J., Virén, A., Kaivosoja, T., Aarinen, A., Salminen, V., Jokiniemi, J., 2017. Operation and Emissions of a Hybrid Stove Fueled by Pellets and Log Wood. Energy & Fuels 31, 1961–1968. doi:10.1021/acs.energyfuels.6b02717

Lampe, U., Gerblinger, J., Meixner, H., 1995. Carbon-monoxide sensors based on thin films of BaSnO3. "Sensors Actuators, B Chem. 24–25, 657–660. doi:10.1016/0925-4005(95)85145-3

Lara-García, H.A., Vera, E., Mendoza-Nieto, J.A., Gómez-García, J.F., Duan, Y., Pfeiffer, H., 2017. Bifunctional application of lithium ferrites (Li5FeO4 and LiFeO2) during carbon monoxide (CO) oxidation and chemisorption processes. A catalytic, thermogravimetric and theoretical analysis. Chem. Eng. J. doi:10.1016/j.cej.2017.06.135

Lask, K., Gadgil, A., 2017. Performance and emissions characteristics of a lighting cone for charcoal stoves. Energy Sustain. Dev. 36, 64-67. doi:10.1016/j.esd.2016.03.001

Launhardt, T., Thoma, H., 2000. Investigation on organic pollutants from a domestic heating system using various solid biofuels. Chemosphere 40, 1149–1157. doi:10.1016/S0045-6535(99)00364-1

Lee, I., Zaera, F., 2014. Catalytic oxidation of carbon monoxide at cryogenic temperatures. doi:10.1016/j.jcat.2014.08.018

Lee, X.J., Lee, L.Y., Gan, S., Thangalazhy-Gopakumar, S., Ng, H.K., 2017. Biochar potential evaluation of palm oil wastes through slow pyrolysis: Thermochemical characterization and pyrolytic kinetic studies. Bioresour. Technol. 236, 236, pp. 155–163. doi:10.1016/j.biortech.2017.03.105

Li, L., Deng, D., Huang, S., Song, H., Xu, K., Zhang, L., Lv, Y., 2018. UV-Assisted Cataluminescent Sensor for Carbon Monoxide Based on Oxygen-Functionalized g-C 3 N 4 Nanomaterials. Anal. Chem. 90, 9598–9605. doi:10.1021/acs.analchem.8b02532

Li, Z., Nan, D., Yuhan, G., 2012. Research on Infrared Carbon Monoxide Monitoring System Based on Least Squares Support Vector Machine, in: International Workshop on Information and Electronics Engineering (IWIEE). pp. 1926–1931. doi:10.1016/j.proeng.2012.01.238

Liao, Y., Jia, L., Chen, R., Gu, O., Sakurai, M., Kameyama, H., Zhou, L., Ma, H., Guo, Y., 2016. Charcoal-supported catalyst with enhanced thermal-stability for the catalytic combustion of volatile organic compounds. doi:10.1016/j.apcata.2016.04.028

Lin, C., Xian, X., Qin, X., Wang, D., Tsow, F., Forzani, E., Tao, N., 2018. High Performance Colorimetric Carbon Monoxide Sensor for Continuous Personal Exposure Monitoring. ACS Sensors 3, 327–333. doi:10.1021/acssensors.7b00722

Lisandy, K.Y., Kim, Gyeong-min, Kim, J., Kim, Gyu-bo, Jeon, C., 2017. Enhanced Accuracy of the Reaction Rate Prediction Model for Carbonaceous Solid Fuel Combustion. doi:10.1021/acs.energyfuels.7b00159

Lucarelli, K., Wyne, K., Svenson, J.E., Lucarelli, K., Wyne, K., Svenson, J.E., 2018. Improved cookstoves and their effect on carbon monoxide levels in San Lucas Tolimán , Guatemala. Int. J. Environ. Health Res. 3123, 1–7. doi:10.1080/09603123.2018.1429575

MacCarty, N., Still, D., Ogle, D., 2010. Fuel use and emissions performance of fifty cooking stoves in the laboratory and related benchmarks of performance. Energy Sustain. Dev. 14, 161-171. doi:10.1016/j.esd.2010.06.002

Maity, A., Ghosh, A., Majumder, S.B., 2016. Engineered spinel-perovskite composite sensor for selective carbon monoxide gas sensing. Sensors Actuators, B Chem. 225, 128–140. doi:10.1016/j.snb.2015.11.025

Malika, A., Jacques, N., Jaafar, E.F., Fatima, B., Mohammed, A., 2016. Pyrolysis investigation of food wastes by TG-MS-DSC technique. Biomass Convers. Biorefinery 6, 161–172. doi:10.1007/s13399-015-0171-9

Malyshev, V. V., Pislyakov, A. V., 2008. Investigation of gas-sensitivity of sensor structures to hydrogen in a wide range of temperature, concentration and humidity of gas medium. Sensors Actuators, B Chem. 134, 913–921. doi:10.1016/j.snb.2008.06.046

Mantananont, N., Patumsawad, S., 2016. Particulate matter and gaseous emission rate from combustion of Thai lignite and agricultural residues in a fixed-bed combustor. Energy Sources, Part A Recover. Util. Environ. Eff. 38, 478–484. doi:10.1080/15567036.2013.783655

Martín-Lara, M.A., Blázquez, G., Ronda, A., Calero, M., 2016. Kinetic study of the pyrolysis of pine cone shell through non-isothermal thermogravimetry: Effect of heavy metals incorporated by biosorption. Renew. Energy 96, 613–624. doi:10.1016/j.renene.2016.05.026

Martín-Lara, M.A., Ronda, A., Blázquez, G., Pérez, A., Calero, M., 2018. Pyrolysis kinetics of the lead-impregnated olive stone by non-isothermal thermogravimetry. Process Saf. Environ. Prot. 113, 448–458. doi:10.1016/j.psep.2017.11.015

Mehetre, S.A., Panwar, N.L., Sharma, D., Kumar, H., 2017. Improved biomass cookstoves for sustainable development : A review. Renew. Sustain. Energy Rev. 73, 672–687. doi:10.1016/j.rser.2017.01.150

Ministry of New and Renewable Energy - India, 2015. Approved Models of Portable Improved Biomass Cookstoves [WWW Document]. Manuf. Improv. Biomass Cookstoves (As 08.07.2015). URL http://mnre.gov.in/file-manager/UserFiles/approved-models-of-portable-improved-biomass-cookstove-manufactures.pdf (accessed 2.13.19).

Moghtaderi, B., Fletcher, D.F., 1998. Flaming Combustion Characteristics of Wood-Based Materials, in: International Association for Fire Safety Science. pp. 209–219.

Mohajeri, A., Hassani, N., 2018. Catalytic activity of corrole complexes with post-transition elements for the oxidation of carbon monoxide: A first-principles study. New J. Chem. doi:10.1039/c8nj01603h

Mokoena, L., Pattrick, G., Scurrell, M.S., 2016. Catalytic activity of gold-perovskite catalysts in the oxidation of carbon monoxide. Gold Bull. doi:10.1007/s13404-016-0180-x

Molavi, R., Sheikhi, M.H., 2018. Low temperature carbon monoxide gas sensor based on Ag-Co3O4 thick film nanocomposite. Mater. Lett. 233, 74–77. doi:10.1016/j.matlet.2018.08.087

Moragues, M.E., Toscani, A., Sancenón, F., Martínez-Máñez, R., White, A.J.P.P., Wilton-Ely, J.D.E.T.E.T., 2014. A chromo-fluorogenic synthetic “canary” for CO detection based on a pyrenylvinyl ruthenium (II) complex. J. Am. Chem. Soc. 136, 11930–11933. doi:10.1021/ja507014a

Mukhopadhyay, R., Sambandam, S., Pillarisetti, A., Jack, D., Mukhopadhyay, K., Balakrishnan, K., Vaswani, M., Bates, N., Kinney, P., Arora, N., Smith, K., Mukhopadhyay, R., Sambandam, S., Pillarisetti, A., Jack, D., Mukhopadhyay, R., Sambandam, S., Pillarisetti, A., Jack, D., Mukhopadhyay, K., Balakrishnan, K.,

Vaswani, M., Bates, M.N., Kinney, P.L., Arora, N., Smith, K.R., 2012. Cooking practices, air quality, and the acceptability of advanced cookstoves in Haryana , India : an exploratory study to inform large-scale interventions. Glob. Health Action 5, 1–13. doi:10.3402/gha.v5i0.19016

Muktham, R., Ball, A.S., Bhargava, S.K., Bankupalli, S., 2016. Study of thermal behavior of deoiled karanja seed cake biomass: Thermogravimetric analysis and pyrolysis kinetics. Energy Sci. Eng. 4, 86–95. doi:10.1002/ese3.109

Mulrooney, J., Clifford, J., Fitzpatrick, C., Chambers, P., Lewis, E., 2008. A mid-infrared optical fibre sensor for the detection of carbon monoxide exhaust emissions. Sensors Actuators, A Phys. 144, 13–17. doi:10.1016/j.sna.2007.12.013

Nagai, D., Nakashima, T., Nishibori, M., Itoh, T., Izu, N., Shin, W., 2013. Thermoelectric gas sensor with CO combustion catalyst for ppm level carbon monoxide detection. Sensors Actuators, B Chem. 182, 789–794. doi:10.1016/j.snb.2013.03.061

Nandy, T., Ronald A. Coutu, J., Ababei, C., 2018. Carbon Monoxide Sensing Technologies for Next-Generation Cyber-Physical Systems. Sensors 18, 1–29. doi:10.3390/s18103443

Nikfarjam, A., Salehifar, N., 2015. UV Enhancement in Carbon Monoxide Detection Using Cu Thin Film on TiO2 Nanofiber Sensor. Sensors Lett. 13, 599-604(6). doi:10.1166/sl.2015.3509

Njenga, M., Iiyama, M., J., Amnadass, R., Helander, H., Larsson, L., De Leeuw, J., Neufeldt, H., Röing De Nowina, K., Sundberg, C., Iiyama, M., Jamnadass, R., Helander, H., Larsson, L., Leeuw, J. De, 2016. Gasifier as a cleaner cooking system in rural Kenya. Clean. Prod. 121, 208-217. doi:10.1016/j.jclepro.2016.01.039

Njenga, M., Mahmoud, Y., Mendum, R., Iiyama, M., Jamnadass, R., De Nowina, K.R., Sundberg, C., 2017. Quality of charcoal produced using micro gasification and how the new cook stove works in rural Kenya. Environ. Res. Lett. 12, art. no. 095001, . doi:10.1088/1748-9326/aa7499

Nussbaumer, T., 2003. Combustion and Co-combus tion of Biomass: Fundamentals, Technologie s, and Primary Measures for Emission Reduction. Energy & Fuels 17, 1510–1521. doi:10.1021/ef030031q

Nuutinen, K., Jokiniemi, J., Sippula, O., Lamberg, H., Sutinen, J., 2014. Effect of air staging on fine particle , dust and gaseous emissions from masonry heaters. Biomass and Bioenergy 67, 167–178. doi:10.1016/j.biombioe.2014.04.033

Nyombi, A., Williams, M.R., Wessling, R., 2019. Toxic emissions from smouldering combustion of woody biomass and derived char with a case study of CO build-up in an ISO container. Energy Sources, Part A Recover. Util. Environ. Eff. doi:10.1080/15567036.2019.1623348

Office-for-National-Statistics-UK, 2016. Number of deaths from accidental poisoning by carbon monoxide, England and Wales, deaths registered in 2011-2015. London.

Okamoto, H., Obayashi, H., Kudo, T., 1980. Carbon monoxide gas sensor made of stabilised Zirconia. Solid State Ionics 1, 319–326. doi:https://doi.org/10.1016/0167-2738(80)90012-0

Oleksenko, L.P., Maksimovich, N.P., Shuvar, L. V, Matushko, I.P., 2013. Nanosized Semiconductor CoxOy/SnO2 Materials for Carbon Monoxide Sensors. Theor. Exp. Chem. 49, 310–314. doi:10.1007/s11237-013-9330-x

Ortega, P.P., Rocha, L.S.R., Cortés, J.A., Ramirez, M.A., Buono, C., Ponce, M.A., Simões, A.Z., 2019. Towards carbon monoxide sensors based on europium doped cerium dioxide. Appl. Surf. Sci. 464, 692–699. doi:10.1016/j.apsusc.2018.09.142

Osman, A.I., Abdelkader, A., Johnston, C.R., Morgan, K., Rooney, D.W., 2017. Thermal Investigation and Kinetic Modeling of Lignocellulosic Biomass Combustion for Energy Production and Other Applications. Ind. Eng. Chem. Res. 56, 12119–12130. doi:10.1021/acs.iecr.7b03478

Otagawa, T., Madou, M., Wing, S., Rich-Alexander, J., Kusanagi, S., Fujioka, T., Yasuda, A., 1990. Planar microelectrochemical carbon monoxide sensors. Sensors Actuators B1 1, 319–325. doi:10.1016/0925-4005(90)80223-m

Ots, R., Heal, M.R., Young, D.E., Williams, L.R., Allan, J.D., Nemitz, E., Green, D.C., Kuenen, J.J.P., Reis, S., Vieno, M., 2018. Modelling carbonaceous aerosol from residential solid fuel burning with different assumptions for emissions 4497–4518.

Ozawa, T., 1965. A New Method of Analyzing Thermogravimetric Data. Bull. Chem. Soc. Jpn. 38, 1881–1886. doi:10.1246/bcsj.38.1881

Ozil, F., Tschamber, V., Haas, F., Trouvé, G., 2009. Efficiency of catalytic processes for the reduction of CO and VOC emissions from wood combustion in domestic fireplaces. Fuel Process. Technol. 90, 1053–1061. doi:10.1016/j.fuproc.2009.03.019

Özsin, G., Pütün, A.E., 2017. Kinetics and evolved gas analysis for pyrolysis of food processing wastes using TGA/MS/FT-IR. Waste Manag. 64, 315-326. doi:10.1016/j.wasman.2017.03.020

Pałaszynska, K., Juszczak, M., 2018. Gaseous emissions during agricultural biomass combustion in a 50 kW moving step grate boiler. Chem. Process Eng. 39, 197–208. doi:10.24425/119109

Paliwal, A., Sharma, A., Tomar, M., Gupta, V., 2017. Carbon monoxide (CO) optical gas sensor based on ZnO thin films. Sensors Actuators, B Chem. 250, 679–685. doi:10.1016/j.snb.2017.05.064

Pannek, C., Tarantik, K.R., Schmitt, K., Wöllenstein, J., 2018. Investigation of gasochromic rhodium complexes towards their reactivity to CO and integration into an optical gas sensor for fire gas detection. Sensors (Switzerland) 18, 1–15. doi:10.3390/s18071994

Park, J.-H., Wang, J.J., Xiao, R., Tafti, N., DeLaune, R.D., Seo, D.-C., 2018. Degradation of Orange G by Fenton-like reaction with Fe-impregnated biochar catalyst. doi:10.1016/j.biortech.2017.10.030

Parker, D.S.N., Kaiser, R.I., Troy, T.P., Kostko, O., Ahmed, M., Mebel, A.M., 2015. Toward the Oxidation of the Phenyl Radical and Prevention of PAH Formation in Combustion Systems. doi:10.1021/jp509170x

Paul, S., Chavan, N.N., Radhakrishnan, S., 2009. Polypyrrole functionalized with ferrocenyl derivative as a rapid carbon monoxide sensor. Synth. Met. 159, 415–418. doi:10.1016/j.synthmet.2008.10.013

Paulsen, A.D., Kunsa, T.A., Carpenter, A.L., Amundsen, T.J., Schwartz, N.R., Harrington, J., Reed, J., Alcorn, B., Gattoni, J., Yelvington, P.E., 2018. Gaseous and particulate emissions from a chimneyless biomass cookstove equipped with a potassium catalyst. Appl. Energy 235, 369–378. doi:10.1016/j.apenergy.2018.10.122

Pérez-Maqueda, L.A., Criado, J.M., 2000. Accuracy of Senum and Yang's approximations to the Arrhenius integral. J. Therm. Anal. Calorim. 60, 909–915. doi:10.1023/A:1010115926340

Petruk, V.G., Kravets, A.G., 2007. Carbon monoxide sensors based on SnOx nanoparticles. Tech. Phys. 52, 231–234. doi:10.1134/s1063784207020132

Phawachalotorn, C., Sanguanruang, O., Ishihara, T., 2012. Highly selective amperometric sensors for carbon monoxide detection in exhaust gas. Sensors Actuators, B Chem. 161, 635–640. doi:10.1016/j.snb.2011.10.081

Phuong, N.H., Ha, N.H., Thach, P.D., Thinh, D.D., Huong, N.T., Hong, H.S., 2017. Fast response of carbon monoxide gas sensors using a highly porous network of ZnO nanoparticles decorated on 3D reduced graphene oxide. Appl. Surf. Sci. 434, 1048–1054. doi:10.1016/j.apsusc.2017.11.047

Poggi, L.A., Singh, K., 2016. Thermal degradation capabilities of modified bio-chars and fluid cracking catalyst (FCC) for acetic acid. doi:10.1016/j.biombioe.2016.04.018

Pope, D., Bruce, N., Dherani, M., Jagoe, K., Rehfuess, E., 2017. Real-life effectiveness of 'improved' stoves and clean fuels in reducing PM2.5 and CO: Systematic review and meta-analysis. Environ. Int. 101, 7–18. doi:10.1016/j.envint.2017.01.012

Prasad, R.M., Gurlo, A., Riedel, R., Hübner, M., Barsan, N., Weimar, U., 2010. Microporous ceramic coated SnO2 sensors for hydrogen and carbon monoxide sensing in harsh reducing conditions. Sensors Actuators, B Chem. 149, 105–109. doi:10.1016/j.snb.2010.06.016

Qiu, X., Wei, Y., Li, N., Guo, A., Zhang, E., Li, C., Peng, Y., Wei, J., Zang, Z., 2019. Development of an early warning fire detection system based on a laser spectroscopic carbon monoxide sensor using a 32-bit system-on-chip. Infrared Phys. Technol. 96, 44–51. doi:10.1016/j.infrared.2018.11.013

Rabaçal, M., Fernandes, U., Costa, M., 2013. Combustion and emission characteristics of a domestic boiler fired with pellets of pine, industrial wood wastes and peach stones. Renew. Energy 51, 220–226. doi:10.1016/j.renene.2012.09.020

Raj, A., Robert, G., Ho, S., 2012. Reaction mechanism for the free-edge oxidation of soot by O2. Combust. Flame 159, 3423–3436. doi:10.1016/j.combustflame.2012.06.004

Raj, A., Yang, S.Y., Cha, D., Tayouo, R., Chung, S.H., 2013. Structural effects on the oxidation of soot particles by O2: Experimental and theoretical study. Combust. Flame 160, 1812–1826. doi:10.1016/j.combustflame.2013.03.010

Rakitskaya, T.L., Kiose, T.A., Ennan, A.A., Golubchik, K.O., Oleksenko, L.P., Gerasiova, V.G., 2016. Effect the conditions of the acid–thermal modification of clinoptilolite have on the catalytic properties of palladium–copper complexes anchored on it in the reaction of carbon monoxide oxidation. Russ. J. Phys. Chem. A. doi:10.1134/S0036024416060182

Rein, G., 2016. Smoldering Combustion, in: Hurley, M.J., Gottuk, D., Hall, J.R., Harada, K., Kuligowski, E., Puchovsky, M., Torero, J., Watts, J.M., Wieczorek, C. (Eds.), SFPE Handbook of Fire Protection Engineering. Springer New York, New York, NY, pp. 581–603. doi:10.1007/978-1-4939-2565-0_19

Rola Mohammad, A.-S., Khaled, M.S., Joydeep, D., 2018. Critical Review of Low-Temperature CO Oxidation and Hysteresis Phenomenon on Heterogeneous Catalysts. Catal. Today 8, 1–19. doi:10.3390/catal8120660

Ross, A.B., Jones, J.M., Chaiklangmuang, S., Pourkashanian, M., Williams, A., Kubica, K., Andersson, J.T., Kerst, M., Danihelka, P., Bartle, K.D., 2002. Measurement and prediction of the emission of pollutants from the combustion of coal and biomass in a fixed bed furnace. Fuel 81, 571–582. doi:10.1016/S0016-2361(01)00157-0

Royer, S., Duprez, D., 2011. Catalytic Oxidation of Carbon Monoxide over Transition Metal Oxides. ChemCatChem 3, 24–65. doi:10.1002/cctc.201000378

Russell, J.B., Jeraci, J.L., 1984. Effect of Carbon Monoxide on Fermentation of Fiber, Starch, and Amino Acids by Mixed Rumen Microorganisms In Vitro. Appl. Environ. Microbiol. 48, 211–217.

Ryan, T.J., Arnold, K.J., 2011. Residential Carbon Monoxide Detector Failure Rates in the United States. Am. J. Public Health 101, 15–17. doi:10.2105/AJPH.2011.300274

Sadaka, S., Liechty, H., Pelkki, M., Blazier, M., 2015. Pyrolysis and combustion kinetics of raw and carbonized cottonwood and switchgrass agroforest. doi:10.15376/biores.10.3.4498-4518

Sajjad, M., Aamer, M., Taha, S., Taqvi, H., 2017. Pyrolysis, kinetics analysis, thermodynamics parameters and reaction mechanism of Typha latifolia to evaluate its bioenergy potential Bioresource Technology. Bioresour. Technol. 245, 491–501. doi:10.1016/j.biortech.2017.08.162

Salehi, A., 2003. A highly sensitive self heated SnO2 carbon monoxide sensor. Sensors Actuators, B Chem. 96, 88–93. doi:10.1016/S0925-4005(03)00490-8

Salker, A. V., Choi, N.J., Kwak, J.H., Joo, B.S., Lee, D.D., 2005. Thick films of In, Bi and Pd metal oxides impregnated in LaCoO3 perovskite as carbon monoxide sensor. Sensors Actuators, B Chem. 106, 461–467. doi:10.1016/j.snb.2004.09.008

Sambandam, S., Balakrishnan, K., Ghosh, S., Sadasivam, A., Madhav, S., Ramasamy, R., Samanta, M., Mukhopadhyay, K., Rehman, H., Ramanathan, V., 2015. Can Currently Available Advanced Combustion Biomass Cook-Stoves Provide Health Relevant Exposure Reductions? Results from Initial Assessment of Select Commercial Models in India. Ecohealth 12, 25–41. doi:10.1007/s10393-014-0976-1

Santhosh, P., Manesh, K.M., Gopalan, A., Lee, K.P., 2007. Novel amperometric carbon monoxide sensor based on multi-wall carbon nanotubes grafted with polydiphenylamine-Fabrication and performance. Sensors Actuators, B Chem. 125, 92–99. doi:10.1016/j.snb.2007.01.044

Savagatrup, S., Schroeder, V., He, X., Lin, S., He, M., Yassine, O., Salama, K.N., Zhang, X.-X., Swager, T.., 2017. Bio-Inspired Carbon Monoxide Sensors with Voltage-Activated Sensitivity. J. Ger. Chem. Soc. 56, 14066–14070. doi:10.1002/anie.201707491

Savage, N.O., Akbar, S.A., Dutta, P.K., 2001. Titanium dioxide based high temperature carbon monoxide selective sensor. Sensors Actuators, B Chem. 72, 239–248. doi:10.1016/S0925-4005(00)00676-6

Schmidl, C., Luisser, M., Padouvas, E., Lasselsberger, L., Rzaca, M., Ramirez-Santa Cruz, C., Handler, M., Peng, G., Bauer, H., Puxbaum, H., 2011. Particulate and gaseous emissions from manually and automatically fired small scale combustion systems. doi:10.1016/j.atmosenv.2011.05.006

Senum, G.I., Yang, R.., 1977. Rational approximations of the intergral of the Arrhenius function. Therm. Anal. 445–447. doi:10.1016/j.ajpath.2011.02.031

Shanying, Z., Youping, C., Gang, Z., Jiming, S., 2010. A near-infrared optical fiber sensor for carbon monoxide concentration monitoring. Microw. Opt. Technol. Lett. 55, 363–366. doi:10.1002/mop

Shen, G., Xue, M., Chen, Y., Yang, C., Li, W., Shen, H., Huang, Y., Zhang, Y., Chen, H., Zhu, Y., Wu, H., Ding, A., Tao, S., 2014. Comparison of carbonaceous particulate matter emission factors among different solid fuels burned in residential stoves. Atmos. Environ. 89, 337–345. doi:10.1016/j.atmosenv.2014.01.033

Sher, F., Pans, M.A., Daniel, T.A., Sun, C., Liu, H., 2017. Experimental investigation of woody and non-woody biomass combustion in a bubbling fluidised bed combustor focusing on gaseous emissions and temperature profiles. Energy 141, 2069–2080. doi:10.1016/j.energy.2017.11.118

Shimizu, Y., Kaneyasu, K., Ueda, T., Goto, T., Hyodo, T., 2016. Potentiometric Carbon Monoxide Sensors Using an Anion-Conducting Polymer Electrolyte and Au-Loaded SnO2 Electrodes. J. Electrochem. Soc. 163, B300–B308. doi:10.1149/2.0561607jes

Shimizu, Y., Yamamoto, S., Takase, S., 2017. A thick-film impedancemetric carbon monoxide sensor using layered perovskite-type cuprate. Sensors Actuators, B Chem. 249, 667–672. doi:10.1016/j.snb.2017.04.059

Sikarwar, V.S., Zhao, M., Fennell, P.S., Shah, N., Anthony, E.J., 2017. Progress in biofuel production from gasification. Prog. Energy Combust. Sci. 61, 189!248. doi:10.1016/j.pecs.2017.04.001

Sin, J.K.., Sharma, R.K., Chan, P.C.., Tang, Z., Yan, G., Hsing, I.-M., 2002. Sensitive, selective and stable tin dioxide thin-films for carbon monoxide and hydrogen sensing in integrated gas sensor array applications. Sensors Actuators B Chem. 72, 160–166. doi:10.1016/s0925-4005(00)00646-8

Song, Y., Chu, X., Lin, Y., Yang, X., 2017. Pyrrolidone Modifying Gold Nanocatalysts for Enhanced Catalytic Activities in Aerobic Oxidation of Alcohols and Carbon Monoxide. J. Chem. doi:10.1155/2017/5257296

Starink, M.J., 2003. The determination of activation energy from linear heating rate experiments: A comparison of the accuracy of isoconversion methods. Thermochim. Acta 404, 163–176. doi:10.1016/S0040-6031(03)00144-8

Still, D., Bentson, S., Li, H., 2015. Results of Laboratory Testing of 15 Cookstove Designs in Accordance with the ISO/IWA Tiers of Performance. Ecohealth 12, 12–24. doi:10.1007/s10393-014-0955-6

Sudarsanam, P., Selvakannan, P.R., Soni, S.K., Bhargava, S.K., Reddy, B.M., 2014. Structural evaluation and catalytic performance of nano-Au supported on nanocrystalline Ce0.9Fe0.1O2-δ solid solution for oxidation of carbon monoxide and benzylamine. doi:10.1039/c4ra07450e

Sun, J., Hoon, S., Jung, S., Ryu, C., Jeon, J., Shin, M., Park, Y., 2016. Production and utilization of biochar : A review. J. Ind. Eng. Chem. 40, 1–15. doi:10.1016/j.jiec.2016.06.002

Suryono, S., Saputra, R., Surarso, B., Bardadi, A., 2017. A web-based wireless sensor system to measure carbon monoxide concentration, in: International Conference on Electrical Engineering, Computer Science and Informatics (EECSI). pp. 19–21. doi:10.1109/EECSI.2017.8239174

Svintsitskiy, D.A., Pakharukov, I.Y., Slavinskaya, E.M., Kardash, T.Y., Parmon, V.N., Boronin, A.I., 2016. Influence of the Copper(II) Oxide Dispersion on its Catalytic Properties in Carbon Monoxide Oxidation: A Comparative Study by Using Two Types of Catalytic Reactors. ChemCatChem. doi:10.1002/cctc.201600802

Tagle, M., Smith, K.R., Pillarisetti, A., Teresa, M., Karin, H., Soares, A., Torres, R., Galeano, A., Oyola, P., Balmes, J., 2018. Monitoring and modeling of household air quality related to use of different Cookfuels in Paraguay. Indoor Air 1–11. doi:10.1111/ina.12513

Tang, C., Zhou, Q., Zhu, S., Zhao, Z., Xu, L., Chen, W., Kumar, R., Gui, Y., 2017. Highly sensitive carbon monoxide (CO) gas sensors based on Ni and Zn doped SnO 2 nanomaterials. Ceram. Int. 44, 4392–4399. doi:10.1016/j.ceramint.2017.12.038

Tang, J.-Y., Shen, J.-S., Chen, L., Jiang, J.-W., Lu, J., Zhao, X., Dai, G.-L., 2018. Investigation of carbon monoxide catalytic oxidation on vanadium-embedded graphene. Monatshefte fur Chemie. doi:10.1007/s00706-018-2181-3

Tess, M.E., Cox, J.A., 1998. Humidity-Independent Solid-State Amperometric Sensor for Carbon Monoxide Based on an Electrolyte Prepared by Sol-Gel Chemistry. Anal. Chem. 70, 187–190. doi:10.1021/ac9708396

Thomazy, D., So, S., Kosterev, A., Lewicki, R., Dong, L., Sani, A.A., Tittel, F.K., 2010. Low-power laser-based carbon monoxide sensor for fire and post-fire detection using a compact Herriott multipass cell, in: Quantum Sensing and Nanophotonic Devices VII. pp. 76080C1-76080C6. doi:10.1117/12.841926

Thurmond, K., Loparo, Z., Partridge, W., Vasu, S.S., 2016. A light-emitting diode- (LED-) based absorption sensor for simultaneous detection of carbon monoxide and carbon dioxide. Appl. Spectrosc. 70, 962–971. doi:10.1177/0003702816641261

Tischner, A., Maier, T., Stepper, C., Köck, A., 2008. Ultrathin SnO2 gas sensors fabricated by spray pyrolysis for the detection of humidity and carbon monoxide. Sensors Actuators, B Chem. 134, 796–802. doi:10.1016/j.snb.2008.06.032

Toscani, A., Mar, Ì., Moragues, Ì.E., Dingwall, P., Brown, N.J., Mart, Û., Çez, Ì., White, A.J.P., Wilton-ely, J.D.E.T., 2015. Ruthenium (II) and Osmium (II) Vinyl Complexes as Highly Sensitive and Selective Chromogenic and Fluorogenic Probes for the Sensing of Carbon Monoxide in Air. Chem. Eur. J. 21, 14529–14538. doi:10.1002/chem.201501843

Trubetskaya, A., Jensen, P.A., Jensen, A.D., Steibel, M., Spliethoff, H., Glarborg, P., Larsen, F.H., 2016. Comparison of high temperature chars of wheat straw and rice husk with respect to chemistry, morphology and reactivity. doi:10.1016/j.biombioe.2016.01.017

Tsai, P.P., Chen, I.C., Tzeng, M.H., 1995. Tin oxide (SnOX) carbon monoxide sensor fabricated by thick-film methods. Sensors Actuators B. Chem. 25, 537–539. doi:10.1016/0925-4005(95)85116-X

Tschamber, V., Trouvé, G., Leyssens, G., Le-Dreff-Lorimier, C., Jaffrezo, J.L.J.-L., Genevray, P., Dewaele, D., Cazier, F., Labbé, S., Postel, S., 2016. Domestic Wood Heating Appliances with Environmental High Performance: Chemical Composition of Emission and Correlations between Emission Factors and Operating Conditions. Energy and Fuels 30, 7241–7255. doi:10.1021/acs.energyfuels.6b00333

Umegaki, T., Inoue, T., Kojima, Y., 2016. Fabrication of hollow spheres of Co3O4 for catalytic oxidation of carbon monoxide. doi:10.1016/j.jallcom.2015.12.001

Van Geloven, P., Honore, M., Roggen, J., Leppavuori, S., Rantala, T., 1991. The influence of relative humidity on the response of tin oxide gas sensors to carbon monoxide. Sensors Actuators B. Chem. 4, 185–188. doi:10.1016/0925-4005(91)80196-Q

Vanderover, J., Oehlschlaeger, M.A., 2010. A mid-infrared scanned-wavelength laser absorption sensor for carbon monoxide and temperature measurements from 900 to 4000 K. Appl. Phys. B Lasers Opt. 99, 353–362. doi:10.1007/s00340-009-3849-5

Vanderover, J., Wang, W., Oehlschlaeger, M.A., 2011. A carbon monoxide and thermometry sensor based on mid-IR quantum-cascade laser wavelength-modulation absorption spectroscopy. Appl. Phys. B Lasers Opt. 103, 959–966. doi:10.1007/s00340-011-4570-8

Varjani, S., Kumar, G., Rene, E.R., 2019. Developments in biochar application for pesticide remediation : Current knowledge and future research directions. J. Environ. Manage. 232, 505–513. doi:10.1016/j.jenvman.2018.11.043

Vlaev, L., Nedelchev, N., Gyurova, K., Zagorcheva, M., 2008. A comparative study of non-isothermal kinetics of decomposition of calcium oxalate monohydrate. J. Anal. Appl. Pyrolysis 81, 253–262. doi:10.1016/j.jaap.2007.12.003

Vyazovkin, S., 2006. Model-free Kinetics: Staying free of multiplying entities without necessity. J. Therm. Anal. Calorim. 83, 45–51.

Vyazovkin, S., Wight, A, C., 1998. Isothermal and non-isotherm al kinetics of therm ally stimulated reactions of solids. Int. Rev. s Phys. Chem. 17, 407–433.

Wan, S., Wu, J., Zhou, S., Wang, R., Gao, B., He, F., 2018. Enhanced lead and cadmium removal using biochar-supported hydrated manganese oxide (HMO) nanoparticles: Behavior and mechanism. doi:10.1016/j.scitotenv.2017.10.188

Wang, C.T., Chen, H.Y., Chen, Y.C., 2013. Gold/vanadium-tin oxide nanocomposites prepared by co-precipitation method for carbon monoxide gas sensors. Sensors Actuators, B Chem. 176, 945–951. doi:10.1016/j.snb.2012.10.041

Wang, C.T., Chen, M.T., 2010. Vanadium-promoted tin oxide semiconductor carbon monoxide gas sensors. Sensors Actuators, B Chem. 150, 360–366. doi:10.1016/j.snb.2010.06.060

Wang, G., Zhang, J., Shao, J., Sun, H., Zuo, H., 2014. Thermogravimetric Analysis of Coal Char Combustion Kinetics. J. Iron Steel Res. Int. 21, 897–904. doi:https://doi.org/10.1016/S1006-706X(14)60159-X

Wang, P., Howard, B.H., 2018. Impact of thermal pretreatment temperatures on woody biomass chemical composition, physical properties and microstructure. Energies 11, 25. doi:10.3390/en11010025

Wang, S., Zhao, Y., Huang, J., Wang, Y., Wu, S., Zhang, S., Huang, W., 2006. Low-temperature carbon monoxide gas sensors based gold/tin dioxide. Solid. State. Electron. 50, 1728–1731. doi:10.1016/j.sse.2006.10.002

Wang, Z., Lin, L., Li, Y., Miao, B., Zeng, W., 2013. Recognition of carbon monoxide with SnO2/Ti thick-film sensor and its gas-sensing mechanism. Sensors Actuators B Chem. 191, 1–8. doi:10.1016/j.snb.2013.09.092

Weber, K., Quicker, P., 2017. Properties of biochar. Fuel 217, 240–261. doi:10.1016/j.fuel.2017.12.054

Wielgosi!nski, G., Łechta!nska, P., Namiecinska, O., 2017. Emission of some pollutants from biomass combustion in comparison to hard coal combustion. J. Energy Inst. 90, 787e796. doi:10.1016/j.joei.2016.06.005

Wilklow-Marnell, M., Jones, W.D., 2017. Catalytic oxidation of carbon monoxide by A-alumina supported 3 nm cerium dioxide nanoparticles. Mol. Catal. doi:10.1016/j.mcat.2017.06.015

Win, K.M., Persson, T., 2014. Emissions from residential wood pellet boilers and stove characterized into start-up, steady operation, and stop emissions. Energy & Fuels 28, 2496–2505. doi:10.1021/ef4016894

Win, K.M., Persson, T., Bales, C., 2012. Particles and gaseous emissions from realistic operation of residential wood pellet heating systems. Atmos. Environ. 59, 320–327. doi:10.1016/j.atmosenv.2012.05.016

Windischmann, H., 2006. A Model for the Operation of a Thin-Film SnO2 Conductance-Modulation Carbon Monoxide Sensor. J. Electrochem. Soc. 126, 627. doi:10.1149/1.2129098

Windischmann, H., Mark, P., 1979. A Model for the Operation of a Thin-Film SnOx Conductance-Modulation Carbon Monoxide Sensor. J. Electrochem. Soc. 126, 627–633. doi:10.1149/1.2129098

Wu, R.J., Wu, J.G., Tsai, T.K., Yeh, C.T., 2006. Use of cobalt oxide CoOOH in a carbon monoxide sensor operating at low temperatures. Sensors Actuators, B Chem. 120, 104–109. doi:10.1016/j.snb.2006.01.053

Xie, S., Dai, H., Deng, J., Yang, H., Han, W., Arandiyan, H., Guo, G., 2014. Preparation and high catalytic performance of Au/3DOM Mn2O3 for the oxidation of carbon monoxide and toluene. doi:10.1016/j.jhazmat.2014.07.033

Xu, T., Huang, H., Luan, W., Qi, Y., Tu, S. tung, 2008. Thermoelectric carbon monoxide sensor using Co-Ce catalyst. Sensors Actuators, B Chem. 133, 70–77. doi:10.1016/j.snb.2008.01.064

Yang, F., Gu, C., Liu, B., Hou, C., Zhou, K., 2019. Pt-activated Ce4La6O17 nanocomposites for formaldehyde and carbon monoxide sensor at low operating temperature. J. Alloys Compd. 787, 173–179. doi:10.1016/j.jallcom.2019.02.066

Yip, F., Christensen, B., Sircar, K., Naeher, L., Bruce, N., Pennise, D., Lozier, M., Pilishvili, T., Loo, J., Stanistreet, D., Nyagol, R., Muoki, J., Beer, L. De, Sage, M., Kapil, V., 2017. Assessment of traditional and improved stove use on household air pollution and personal exposures in rural western Kenya. Environ. Int. 99, 185–191. doi:10.1016/j.envint.2016.11.015

Yu, I.K.M., Tsang, D.C.W., Yip, A.C.K., Chen, S.S., Wang, L., Ok, Y.S., Poon, C.S., 2017. Catalytic valorization of starch-rich food waste into hydroxymethylfurfural (HMF): Controlling relative kinetics for high productivity. doi:10.1016/j.biortech.2017.01.017

Zaikin, V.A., Chakhunashvili, G.B., Koltypin, E.A., Eryshkin, A.V., Vasiliev, A.A., Buturlin, A.I., Malyshev, V.V., Shubin, Y.I., 2002. Gas sensitivity of SnO2 and ZnO thin-film resistive sensors to hydrocarbons, carbon monoxide and hydrogen. Sensors Actuators B Chem. 10, 11–14. doi:10.1016/0925-4005(92)80004-h

Zajac, G., Szyszlak-Barglowicz, J., Slowik, T., Wasilewski, J., Kuranc, A., 2017. Emission characteristics of biomass combustion in a domestic heating boiler fed with wood and Virginia mallow pellets. Fresenius Environ. Bull. 26, 4663–4670.

Zhang, G., Tai, H., Xie, G., Jiang, Y., Zhou, Y., 2013. A carbon monoxide sensor based on single-walled carbon nanotubes doped with copper chloride. Sci. China Technol. Sci. 56, 2576–2580. doi:10.1007/s11431-013-5337-8

Zhang, R., Lu, K., Zong, L., Tong, S., Wang, X., Zhou, J., Lu, Z.-H., Feng, G., 2017. Control synthesis of CeO2 nanomaterials supported gold for catalytic oxidation of carbon monoxide. Mol. Catal. doi:10.1016/j.mcat.2017.09.024

Zhang, W., Wu, F., Li, J., You, Z., 2017. Dispersion–precipitation synthesis of highly active nanosized Co3O4 for catalytic oxidation of carbon monoxide and propane. doi:10.1016/j.apsusc.2017.03.162

Zhi, M., Koneru, A., Yang, F., Manivannan, A., Li, J., Wu, N., 2012. Electrospun La0.8Sr0.2MnO3 nanofibers for a high-temperature electrochemical carbon monoxide sensor. Nanotechnology 23. doi:10.1088/0957-4484/23/30/305501

Zhou, B., Yu, L., Song, H., Li, Y., Zhang, P., Guo, B., Duan, E., 2015. Adsorption and oxidation of SO2 in a fixed-bed reactor using activated carbon produced from oxytetracycline bacterial residue and impregnated with copper. doi:10.1080/10962247.2014.981318

Zhu, L., Zheng, Y., Jian, J., 2015. Effect of palladium oxide electrode on potentiometric sensor response to carbon monoxide. Ionics (Kiel). 21, 2919–2926. doi:10.1007/s11581-015-1487-y

Zhu, S., Chen, Y., Zhang, G., Sa, J., 2010. An optical fiber sensor based on absorption spectroscopy for carbon monoxide detection, in: 2010 International Conference on Computer Design and Applications, ICCDA 2010. pp. 1–4. doi:10.1109/ICCDA.2010.5541304

Zhuiykov, S., 2008. Carbon monoxide detection at low temperatures by semiconductor sensor with nanostructured Au-doped CoOOH films. Sensors Actuators, B Chem. 129, 431–441. doi:10.1016/j.snb.2007.08.046